

1 **Reovirus infection is regulated by NPC1 and endosomal**  
2 **cholesterol homeostasis**

3  
4 Paula Ortega-Gonzalez,<sup>1,2,3,4</sup> Gwen Taylor,<sup>3,4</sup> Rohit K. Jangra,<sup>5,†</sup> Raquel Tenorio,<sup>1</sup>  
5 Isabel Fernández de Castro,<sup>1</sup> Bernardo A. Mainou,<sup>6,††</sup> Robert C. Orchard,<sup>7</sup> Craig B.  
6 Wilen,<sup>8</sup> Pamela H. Briggleb,<sup>3,9</sup> Jorna Sojati,<sup>3,9</sup> Kartik Chandran,<sup>5</sup> Cristina Risco,<sup>1,\*</sup> and  
7 Terence S. Dermody,<sup>3,4,9,\*</sup>

8  
9 <sup>1</sup>Cell Structure Laboratory, National Center for Biotechnology, CNB-CSIC, campus  
10 UAM, Cantoblanco, 28049 Madrid, Spain

11  
12 <sup>2</sup>PhD Program in Molecular Biosciences, Autonoma de Madrid University, 28049  
13 Madrid, Spain

14  
15 <sup>3</sup>Department of Pediatrics, University of Pittsburgh School of Medicine, Pittsburgh,  
16 Pennsylvania, USA

17  
18 <sup>4</sup>Institute of Infection, Inflammation, and Immunity, UPMC Children's Hospital of  
19 Pittsburgh, Pittsburgh, Pennsylvania, USA

20  
21 <sup>5</sup>Department of Microbiology and Immunology, Albert Einstein College of Medicine,  
22 Bronx, New York, USA

23  
24 <sup>6</sup>Department of Pediatrics, Vanderbilt University School of Medicine, Nashville,  
25 Tennessee, USA

26

27   <sup>7</sup>Department of Immunology, University of Texas Southwestern Medical Center, Dallas,  
28   Texas, USA

29

30   <sup>8</sup>Departments of Laboratory Medicine and Immunobiology, Yale University School of  
31   Medicine, New Haven, Connecticut, USA

32

33   <sup>9</sup>Department of Microbiology and Molecular Genetics, University of Pittsburgh School of  
34   Medicine, Pittsburgh, Pennsylvania, USA

35

36   <sup>†</sup>Current address: Department of Microbiology and Immunology, Louisiana State  
37   University Health Sciences Center Shreveport, Shreveport, Louisiana, USA

38

39   <sup>††</sup>Current address: Centers for Disease Control and Prevention, Atlanta, Georgia, USA

40

41   \*Corresponding authors: [crisco@cnb.csic.es](mailto:crisco@cnb.csic.es) and [terence.dermody@chp.edu](mailto:terence.dermody@chp.edu)

42

43   **Running title:** Reovirus infection is regulated by NPC1 and endosomal cholesterol  
44   homeostasis

45 **Abstract**

46 Cholesterol homeostasis is required for the replication of many viruses, including Ebola  
47 virus, hepatitis C virus, and human immunodeficiency virus-1. Niemann-Pick C1 (NPC1)  
48 is an endosomal-lysosomal membrane protein involved in cholesterol trafficking from  
49 late endosomes and lysosomes to the endoplasmic reticulum. We identified NPC1 in  
50 CRISPR and RNA interference screens as a putative host factor for infection by  
51 mammalian orthoreovirus (reovirus). Following internalization via clathrin-mediated  
52 endocytosis, the reovirus outer capsid is proteolytically removed, the endosomal  
53 membrane is disrupted, and the viral core is released into the cytoplasm where viral  
54 transcription, genome replication, and assembly take place. We found that reovirus  
55 infection is significantly impaired in cells lacking NPC1, but infection is restored by  
56 treatment of cells with hydroxypropyl- $\beta$ -cyclodextrin, which binds and solubilizes  
57 cholesterol. Absence of NPC1 did not dampen infection by infectious subvirion  
58 particles, which are reovirus disassembly intermediates that bypass the endocytic  
59 pathway for infection of target cells. NPC1 is not required for reovirus attachment to the  
60 plasma membrane, internalization into cells, or uncoating within endosomes. Instead,  
61 NPC1 is required for delivery of transcriptionally active reovirus core particles into the  
62 cytoplasm. These findings suggest that cholesterol homeostasis, ensured by NPC1  
63 transport activity, is required for reovirus penetration into the cytoplasm, pointing to a  
64 new function for NPC1 and cholesterol homeostasis in viral infection.

65 **Author summary**

66 Genetic screens are useful strategies to identify host factors required for viral infection.  
67 NPC1 was identified in independent CRISPR and RNA interference screens as a  
68 putative host factor required for reovirus replication. We discovered that NPC1-  
69 mediated cholesterol transport is dispensable for reovirus attachment, internalization,  
70 and disassembly but required for penetration of the viral disassembly intermediate from  
71 late endosomes into the cytoplasm. These findings pinpoint an essential function for  
72 cholesterol in the entry of reovirus and raise the possibility that cholesterol homeostasis  
73 regulates the entry of other viruses that penetrate late endosomes to initiate replication.

74

75 **INTRODUCTION**

76 Viral replication is dependent on cellular proteins and pathways for entry, transport, and  
77 release of the viral genome to sites of replication in the cell. Viral attachment to host  
78 cells occurs by interactions with cell-surface proteins, lipids, and carbohydrate moieties  
79 at the plasma membrane and often triggers virus uptake by receptor-mediated  
80 endocytosis (1-7). Viruses that traverse through endosomes must escape the  
81 endosomal compartment and release their genomes at sites of replication to initiate  
82 productive infection. Enveloped viruses generally accomplish endosomal escape using  
83 mechanisms involving receptor- or pH-mediated fusion of the viral envelope and  
84 endosomal membrane (6, 8-10). In contrast, nonenveloped viruses penetrate  
85 endosomal membranes by establishing small membrane pores or large membrane  
86 disruptions (9, 11-13). While both enveloped and nonenveloped viruses depend on  
87 conformational changes of viral structural proteins to escape endosomes, mechanisms  
88 underlying nonenveloped virus membrane penetration are not well understood (6).

89 Mammalian orthoreoviruses (reoviruses) are nonenveloped icosahedral viruses  
90 that infect a broad range of mammalian hosts. Reovirus infections are usually  
91 asymptomatic in humans, but these viruses have been implicated in development of  
92 celiac disease (14). Reovirus virions include two protein shells, the outer capsid,  
93 composed primarily of  $\mu 1-\sigma 3$  heterohexamers, and core (15-17). The core contains 10  
94 segments of double-stranded (ds) RNA, which are classified by size into three large (L),  
95 three medium (M), and four small (S) segments (17). Following receptor-mediated  
96 endocytosis, the reovirus outer capsid undergoes a series of conformational changes  
97 and disassembly events required for release of transcriptionally active cores into the  
98 cytoplasm (18, 19).

99        Within late endosomes, acid-dependent cathepsin proteases catalyze proteolysis  
100      of the viral outer-capsid protein  $\sigma$ 3 and cleavage of the membrane-penetration protein  
101       $\mu$ 1 to  $\delta$  and  $\varphi$ , resulting in formation of metastable intermediates termed infectious  
102      subvирion particles (ISVPs) (20-24). Endosomal lipid composition induces ISVPs to  
103      undergo additional conformational changes resulting in exposure of hydrophobic  
104      domains of  $\delta$ , release of pore-forming fragment  $\mu$ 1N, and formation of ISVP\* $s$  (25, 26).  
105      Release of  $\mu$ 1N during ISVP-to-ISVP\* conversion leads to endosomal penetration and  
106      liberation of the viral core into the cytoplasm where infection progresses (27-31).  
107      Although some essential viral and host factors required for reovirus penetration of the  
108      endosome are known, the process is still not well understood.

109        In this study, we used CRISPR and RNA interference screens to discover that  
110      Niemann Pick C1 (NPC1), an endolysosomal transmembrane protein that mediates  
111      cholesterol egress from late endosomes for redistribution to cellular membranes (32-  
112      34), is required for reovirus infection. We found that genetic ablation of NPC1 in human  
113      brain microvascular endothelial cells (HBMECs) diminishes reovirus infection by virions  
114      but not by ISVPs, suggesting that NPC1 is required for steps that differ between virions  
115      and ISVPs. Treatment of NPC1-null HBMECs with hydroxypropyl-beta-cyclodextrin  
116      (H $\beta$ CD), a macrocycle that binds and solubilizes cholesterol, restored infectivity by  
117      reovirus virions, suggesting that endosomal cholesterol homeostasis contributes to  
118      efficient reovirus entry. While NPC1 is not required for viral attachment to the plasma  
119      membrane, internalization, or uncoating within endosomes, we found that NPC1 is  
120      required for efficient release of reovirus cores from endosomes into the cytoplasm.  
121      Together, these findings suggest that cholesterol homeostasis, mediated by NPC1  
122      cholesterol transport activity, is essential for reovirus cell entry and penetration into the  
123      cytoplasm.

124 **RESULTS**

125 **CRISPR/Cas-9 and siRNA screens for host factors required for reovirus infection**  
126 **identify NPC1**

127 To discover host factors required for reovirus infection, we conducted genome-wide  
128 CRISPR/Cas-9 and siRNA-based cell-survival screens. The CRISPR/Cas-9 screen was  
129 conducted using BV2 mouse microglial cells with the murine Asiago sgRNA library  
130 targeting over 20,000 genes. BV2 CRISPR cell libraries were infected with reovirus  
131 strains type 1 Lang (T1L) and type 3 Dearing (T3D) and cultured for nine days prior to  
132 isolation of genomic DNA (gDNA) from surviving cells and deep sequencing. STARS  
133 analysis was conducted to identify enriched CRISPR gRNAs within the surviving cell  
134 population (Fig. 1A and Table S1). The siRNA screen was conducted using HeLa S3  
135 cells transfected with the ON-TARGET plus siRNA whole genome library targeting over  
136 18,000 genes (35). Transfected cells were infected with reovirus strain T3SA+ and  
137 scored for viability using an ATP-dependent luminescence assay. T3SA+ contains nine  
138 genes from T1L and the S1 gene from strain T3C44-MA (36). T3SA+ binds all known  
139 reovirus receptors and is cytolytic. Robust Z scores (median absolute deviation) were  
140 calculated for each sample (Fig. 1B and Table S2).

141 Key genes and pathways essential for reovirus replication were defined by  
142 comparing the CRISPR/Cas-9 and siRNA screen lists using STRING-db (Fig. 1C). In  
143 the CRISPR/Cas-9 screen, four functional pathways defined by Gene Ontology (GO)  
144 terms were common to both T1L and T3D, including sialic acid biosynthesis and  
145 metabolism (Fig. 1D). Sialic acid is a reovirus attachment factor, and genes involved in  
146 sialic acid biosynthesis and metabolism, including *Slc35a1*, are required for T3SA+  
147 replication in BV2 cells (37). These data provide confidence that the target genes  
148 identified in the CRISPR/Cas-9 screen represent biologically significant candidates. We

149 also compared KEGG pathways identified in the CRISPR/Cas-9 and siRNA screens to  
150 increase the likelihood of significant gene targets. Ribosome and lysosome pathways  
151 were the only pathways common to both screens (Fig. 1E). Lysosomal genes include  
152 *Ctsl*, *Neu1*, and *Npc1*. *Ctsl* encodes cathepsin L, which is required for cleavage of the  
153 reovirus outer capsid to form ISVPs (22). *Neu1* encodes neuraminidase, a lysosomal  
154 sialidase that cleaves sialic acid linkages required for reovirus infectivity (38). *Npc1*  
155 encodes NPC1, a cholesterol transporter that resides in the limiting membrane of  
156 endosomes and lysosomes (33, 34).

157

### 158 **Engineering and characterization of HBMECs with CRISPR-targeted *Npc1***

159 Based on the function of NPC1 in cell entry and replication of other viruses (39) and its  
160 identification in both CRISPR and siRNA screens, we evaluated a potential role for  
161 NPC1 in reovirus replication. Human brain microvascular endothelial cells (HBMECs)  
162 are susceptible to reovirus infection (40) and amenable to CRISPR/Cas-9 gene editing  
163 (41). To facilitate these studies, we used CRISPR/Cas-9 gene editing to engineer a  
164 clonal HBMEC cell line lacking the *NPC1* gene (KO cells). The NPC1 KO cells were  
165 complemented by stable transfection of a functional NPC1 allele (KO+ cells).

166 The newly engineered NPC1 KO and KO+ cell lines were characterized for  
167 NPC1 expression and cholesterol distribution relative to wild-type (WT) HBMECs.  
168 Expression of NPC1 in WT, KO, and KO+ cells was tested using immunoblotting. As  
169 anticipated, NPC1 expression in KO cells was abrogated relative to WT and KO+ cells  
170 (Fig. S1A). There was an observable increase in NPC1 expression in KO+ cells  
171 compared with WT cells (Fig. S1B), but the difference was not statistically significant. In  
172 the absence of functional NPC1, cholesterol reorganizes from a homogeneous  
173 distribution to accumulate in endosomal compartments (32, 33). To define the

174 distribution of cholesterol in NPC1-null HBMECs, we used fluorescent filipin III to label  
175 cholesterol in fixed cells and imaged cholesterol distribution using fluorescence  
176 microscopy (Fig. S1C). Cholesterol distribution was homogeneous in WT (Fig. S1C,  
177 left) and KO+ cells (Fig. S1C, right). However, cholesterol accumulated around the  
178 nucleus in KO cells (Fig. S1C, center) in a pattern consistent with the distribution of  
179 endosomes (Fig. S1D), confirming the absence of functional NPC1. Thus, KO cells  
180 display the expected phenotype of altered cholesterol distribution when NPC1-  
181 dependent cholesterol transport is disrupted. Furthermore, complementing NPC1  
182 expression in KO cells restores the normal distribution of cholesterol, demonstrating  
183 that the observed phenotype is specific for NPC1 expression.

184

#### 185 **Reovirus infection by virions but not by ISVPs is impaired in NPC1 KO cells**

186 ISVPs prepared by treatment of virions *in vitro* with intestinal or endosomal proteases  
187 bind to reovirus receptors and enter target cells by direct penetration of the plasma  
188 membrane and bypass requirements for internalization into the endocytic compartment  
189 and acid-dependent proteolysis (21, 22, 42). To determine whether NPC1 is required  
190 for reovirus replication, and further whether NPC1 mediates a step in the infectious  
191 cycle that differs between virions and ISVPs, we adsorbed WT, KO, and KO+ cells with  
192 reovirus strain T1L M1 P208S virions or ISVPs. Reovirus T1L M1-P208S contains a  
193 point mutation in the M1 gene that causes viral factories to have a globular morphology  
194 similar to the morphology of factories formed by reovirus T3D (43), which renders  
195 infected cells easier to detect. Infected cells were visualized by immunofluorescence  
196 (IF) staining for reovirus antigen at 18 h post-adsorption (Fig. 2). Following adsorption  
197 with reovirus virions, the number of infected KO cells was reduced by approximately  
198 50% relative to infected WT and KO+ cells (Fig. 2A). A similar reduction in the number

199 of infected KO cells relative to WT and KO+ cells was observed when WT, KO, and  
200 KO+ cells were adsorbed with T1L, T3D, and T3SA+ virions, the reovirus strains used  
201 in the CRISPR/Cas9 and siRNA screens (Fig. S2). In contrast, no significant differences  
202 in numbers of infected cells were observed following adsorption of WT, KO, and KO+  
203 cells with ISVPs (Fig. 2B). Viral progeny production and release was determined by  
204 quantifying viral titers in cell lysates and supernatants at 0, 24, and 48 h following  
205 adsorption of WT, KO, and KO+ cells with virions or ISVPs. Following infection by  
206 virions, viral titers in lysates and supernatants of KO cells were 10- to 100-fold less than  
207 those in WT and KO+ cells (Fig. 2C and E). In contrast, following infection by ISVPs,  
208 viral titers in lysates and supernatants of all three cell types were comparable (Fig. 2D  
209 and F). Together, these results suggest that NPC1 is required for reovirus infection and  
210 functions at a step in the infectious cycle that differs between virions and ISVPs.

211

212 **NPC1 is not required for reovirus attachment, internalization, or uncoating**

213 Reovirus entry can be divided into four main stages: viral binding to cell-surface  
214 receptors, viral internalization by endocytosis, proteolytic removal of the viral outer  
215 capsid, and penetration of the core from late endosomes into the cytosol (19). We  
216 characterized NPC1 KO cells for the capacity to support each step of the reovirus entry  
217 pathway to define the function of NPC1 in reovirus infection. To determine whether  
218 NPC1 is required for reovirus attachment to target cells, we quantified viral binding  
219 using flow cytometry. The quantity of virus bound to the surface of all three cell types  
220 was comparable, and no statistically significant differences were observed (Fig. 3A).  
221 These data suggest that reovirus attachment to cells is not dependent on expression of  
222 NPC1.

223 To determine whether NPC1 is required for reovirus to access the endocytic  
224 pathway of target cells, WT, KO, and KO+ cells were adsorbed with fluorescently-  
225 labeled reovirus particles and monitored for reovirus uptake using live-cell imaging. We  
226 found that the kinetics of reovirus internalization into WT, KO, and KO+ cells were  
227 comparable. High-magnification videos (Videos 1, 2, and 3) along with static images  
228 obtained at different intervals (Fig. 3B) demonstrate that attached reovirus particles  
229 internalize slowly in the first ~ 0 - 10 min post-adsorption. During this time, reovirus  
230 particles remain in the periphery, with a few particles coalescing to form large  
231 fluorescent puncta. Convergence of immunofluorescent signals suggests co-transport  
232 of multiple viral particles in the same endocytic compartment, similar to that observed  
233 during reovirus entry into neurons (44). After ~ 15 min post-adsorption, we observed  
234 rapid recruitment of almost every fluorescent puncta to the perinuclear region.

235 To more precisely define the movement of reovirus virions during entry, we  
236 analyzed the trajectories of individual fluorescent virions in Videos 1, 2, and 3 over 36  
237 min using the Spot detector plugin function from Icy software. Trajectory colors change  
238 over time in which each color corresponds to an interval of ~ 7.5 min in the time-lapse  
239 videos (Videos 4, 5, and 6). Analysis of the time-dependent trajectories confirms  
240 observations made in the live-imaging videos. Thus, video-microscopic analysis  
241 demonstrates that reovirus virions are internalized rapidly into HBMECs and that virion  
242 uptake into the endocytic pathway is not impaired in the absence of NPC1.

243 Following internalization of reovirus virions, acid-dependent cathepsin proteases  
244 in late endosomes catalyze disassembly. During disassembly, proteolytic cleavage of  
245 the outermost capsid protein,  $\sigma$ 3, exposes the membrane-penetration protein,  $\mu$ 1, which  
246 is subsequently cleaved to form a variety of intermediates that lead to penetration of the  
247 core particle into the cytoplasm (20-24, 27-30). Cells lacking NPC1 have increased

248 endosomal pH and decreased cathepsin activity (45), which could impair reovirus  
249 uncoating. To determine whether NPC1 is required for reovirus disassembly, we  
250 defined the kinetics of reovirus outer-capsid proteolysis in WT, KO, and KO+ cells by  
251 following the formation of the  $\delta$  cleavage fragment of the  $\mu 1$  protein. Cells were  
252 adsorbed with reovirus virions, and viral proteins in cell lysates were visualized by  
253 immunoblotting at 0, 1, 2, and 3 h post-adsorption using a reovirus-specific antiserum.  
254 No significant differences in the kinetics of  $\mu 1$  proteolysis were observed, with an initial  
255  $\delta$  cleavage product detected 2 h after adsorption in WT, KO, and KO+ cells (Fig. 3C).  
256 These data suggest that the cathepsins that catalyze reovirus disassembly are not  
257 impaired in NPC1 KO HBMECs. Collectively, these results demonstrate that NPC1 is  
258 not required for reovirus receptor binding, internalization, or disassembly.

259

260 **Escape of reovirus cores from endosomes is impaired in cells lacking NPC1**  
261 To determine whether NPC1 is required for escape of reovirus cores into the cytoplasm  
262 following disassembly in the endocytic compartment, we imaged cores in fixed cells by  
263 IF. Cells were adsorbed with fluorescently labeled reovirus virions and incubated in the  
264 presence of cycloheximide for 8 h post-adsorption to inhibit synthesis of new viral  
265 proteins and thus ensure detection of proteins from infecting viral particles. Cells were  
266 stained with a CD-63-specific antibody to label endosomes and an antiserum specific  
267 for reovirus cores and imaged using confocal microscopy. Small puncta consistent with  
268 reovirus cores were observed in WT and KO+ cells, while in KO cells, cores appeared  
269 to accumulate in larger puncta corresponding to endosomes (Fig. 4A). The distribution  
270 of virions, cores, and endosomes was determined to quantify the extent of  
271 colocalization. The results demonstrate frequent colocalization of cores and endosomes  
272 in KO cells (Manders coefficient [Mc]: ~ 0.7), while there was much less colocalization

273 of cores and endosomes in WT and KO+ cells (Mc: ~ 0.3) (Fig. 4B). Colocalization of  
274 virions and cores also was more frequent in KO cells (Mc: ~ 0.45) than in WT (Mc:  
275 ~0.15) or KO+ (Mc: ~0.2) cells, whereas colocalization of virions and endosomes was  
276 comparable in all cell types (Mc: ~ 0.6). These data suggest that cores escape from  
277 endosomes more efficiently in the presence of NPC1.

278 To complement the imaging experiments, we quantified newly synthesized viral  
279 s4 mRNA using RT-qPCR. WT, KO, and KO+ cells were adsorbed with reovirus, RNA  
280 was isolated, and s4 transcripts were quantified at 0, 6, 12, and 24 h post-adsorption.  
281 We observed a statistically significant increase in total s4 RNA in WT and KO+ cells at  
282 12 and 24 h post-adsorption relative to KO cells (Fig. 5). Together, these results  
283 suggest that NPC1 is required for release of transcriptionally active reovirus cores from  
284 endosomes into the cytoplasm.

285  
286 **Cholesterol homeostasis is required for reovirus entry**

287 We thought it possible that NPC1 could serve as an endosomal receptor for reovirus  
288 and interact with one or more viral capsid proteins to enable core delivery into the  
289 cytoplasm, analogous to the function of NPC1 in Ebola virus infection (46, 47).  
290 Alternatively, NPC1 might be required to maintain an endosomal environment with  
291 appropriate cholesterol levels to allow cores to penetrate endosomes. To distinguish  
292 between these possibilities, we tested whether hydroxypropyl- $\beta$ -cyclodextrin (H $\beta$ CD), a  
293 cyclic oligosaccharide that triggers cholesterol release from the endo-lysosomal  
294 compartment (48, 49) and has been used to treat persons with Niemann-Pick disease  
295 type C (50, 51), for the capacity to overcome the effects of NPC1 deficiency on reovirus  
296 infection. To determine whether H $\beta$ CD treatment redistributes cholesterol from  
297 endosomal membranes to a homogeneous distribution in the absence of NPC1, NPC1

298 KO HBMECs were treated with 1 mM H $\beta$ CD, a non-toxic concentration (Fig. S3A), or  
299 PBS for 48 h prior to staining for the filipin III complex. Cells displaying cholesterol  
300 accumulation were distinguished from those with widely distributed cholesterol by  
301 quantifying the mean fluorescence intensity (MFI) of filipin III complex staining. Using  
302 this approach, an increase in MFI correlates with an increase in cholesterol  
303 accumulation. After H $\beta$ CD treatment, KO cells displayed a significant redistribution of  
304 cholesterol, reducing its accumulation in endosomes and enhancing its distribution  
305 broadly throughout the cell, correlating with a statistically significant decrease in MFI  
306 (Fig. S3B,C). These data demonstrate that H $\beta$ CD treatment promotes cholesterol efflux  
307 in KO cells, resulting in a cholesterol-distribution phenotype comparable to WT and  
308 KO+ cells (Fig. S3C).

309 Once we observed that H $\beta$ CD treatment effectively redistributes cholesterol in  
310 KO cells and, thus, functionally complements NPC1 deficiency, we tested whether the  
311 reovirus entry defect in KO cells is due to the absence of NPC1 or impaired cholesterol  
312 homeostasis. WT, KO, and KO+ cells were pre-treated with 1 mM H $\beta$ CD or PBS for 24  
313 h, adsorbed with reovirus virions or ISVPs, and scored for reovirus infection by  
314 immunostaining. Remarkably, H $\beta$ CD treatment rescued infection of KO cells by reovirus  
315 virions (Fig. 6) but did not appreciably affect infection of WT or KO+ cells. H $\beta$ CD  
316 treatment also did not affect infection of WT, KO, or KO+ cells by ISVPs. These data  
317 demonstrate that endosomal cholesterol homeostasis regulates reovirus entry by  
318 enhancing penetration of reovirus core particles into the cytoplasm.

319 **DISCUSSION**

320 In this study, we identified NPC1 as a putative host factor required for reovirus infection  
321 using genome-wide CRISPR/Cas9 and siRNA-based cell-survival screens. NPC1 is an  
322 endolysosomal cholesterol transporter that mediates cholesterol homeostasis (32-34).  
323 Disruption of NPC1 results in cholesterol accumulation in late endosomes (Sup. Fig.  
324 2C) and leads to Niemann-Pick disease type C, an autosomal-recessive  
325 neurodegenerative disorder (32). Early steps in reovirus infection, including receptor  
326 binding, acid-dependent proteolytic disassembly, and ISVP-to-ISVP\* conversion have  
327 been well characterized (19). However, penetration of endosomal membranes and  
328 release of viral cores into the cytoplasm are poorly understood processes. We used  
329 CRISPR/Cas9 gene-targeted HBMECs lacking NPC1 expression to study the function  
330 of NPC1 in reovirus infection. We discovered that NPC1 is dispensable for viral binding  
331 to cell-surface receptors (Fig. 3A), internalization of viral particles (Fig. 3B), and  
332 disassembly of the viral outer capsid (Fig. 3C). However, NPC1 is required for efficient  
333 penetration of reovirus cores into the cytoplasm (Fig. 4). Treatment with H $\beta$ CD reduces  
334 cholesterol accumulation in endosomes (Sup. Fig. 3B and 3C) and restores reovirus  
335 infectivity in NPC1 KO cells (Fig. 6). These findings suggest that regulation of  
336 cholesterol in endosomal compartments is essential for reovirus entry into host cells.

337 NPC1 is required for the replication of several enveloped viruses. The filoviruses  
338 Ebola virus and Marburg virus use NPC1 as an intracellular receptor (46, 47). NPC1  
339 also functions in enveloped virus replication by maintaining cholesterol homeostasis.  
340 Disruption of cholesterol homeostasis by inhibiting NPC1 prevents entry and replication  
341 of dengue virus (52) and African swine fever virus (53) and impairs exosome-dependent  
342 release of hepatitis C virus (54). Additionally, NPC1 has been implicated in cell entry of  
343 quasi-enveloped forms of hepatitis A virus and hepatitis E virus (55, 56). However,

344 NPC1 had not been previously appreciated to function in the replication of a  
345 nonenveloped virus.

346 We found that reovirus binding, internalization, and uncoating do not require  
347 NPC1, suggesting that NPC1 does not function as an intracellular receptor for reovirus.  
348 Instead, we found that cholesterol accumulation in the endocytic pathway diminishes  
349 the efficiency of reovirus core release into the cytoplasm. Using confocal microscopy,  
350 we visualized and quantified the distribution of fluoresceinated reovirus virions, reovirus  
351 cores, and late endosomes in infected cells (Fig. 4). Reovirus cores accumulate in the  
352 lumen of late endosomes in KO cells (Fig. 4A), while virions distribute to endosomes  
353 comparably in WT, KO, and KO+ (Fig. 4B). These findings suggest that cores do not  
354 escape from endosomes efficiently in the absence of NPC1. RNA synthesis, which  
355 occurs in the cytoplasm following release of cores from late endosomes, also was  
356 reduced in KO cells relative to WT and KO+ cells (Fig. 5), providing evidence that core  
357 escape from endosomes is required for initiation of transcription. It is not apparent how  
358 cholesterol accumulation in KO cells blocks core release from late endosomes.

359 In Niemann-Pick disease type C, disruption of cholesterol homeostasis causes  
360 changes in lipid composition of endosomal membranes (57, 58), inverting the ratio of  
361 phosphatidyl choline (PC) and phosphatidyl ethanolamine (PE). The change in PC:PE  
362 ratio may alter mechanical properties of endosomal membranes by inhibiting intra-  
363 endosomal membrane dynamics to favor negative curvature (57, 59). Membrane  
364 composition and dynamics can influence viral entry. Negative membrane curvature  
365 induced by addition of PE or the action of interferon-induced transmembrane protein 3  
366 (IFITM3) impairs adenovirus protein VI-mediated membrane disruption (60) and  
367 enveloped virus fusion (61), respectively. Although reovirus virions are nonenveloped,  
368 entry of reovirus into cells also is inhibited by IFITM3 (62). Many nonenveloped viruses

369 use membrane-modifying proteins with the capacity to interact, destabilize, and disrupt  
370 membranes to mediate genome release into the cytoplasm (12, 63). However, the role  
371 of specific lipids in these processes is not well defined.

372 During reovirus entry, ISVP-to-ISVP\* conversion leads to release of  
373 myristoylated  $\mu$ 1N, which interacts with late endosomal membranes to facilitate release  
374 of cores into the cytoplasm (20-24). PE and PC concentrations in liposomes influence  
375 the efficiency of ISVP-to-ISVP\* conversion (25). Therefore, it is possible that changes in  
376 membrane fluidity, width, or curvature caused by inversion of endosomal membrane  
377 PC:PE ratio in NPC1 KO cells impedes membrane insertion of  $\mu$ 1N or formation and  
378 expansion of the penetration pore. Additionally, accumulation of cholesterol within the  
379 endosomal compartment of NPC1 KO cells could limit recruitment of ISVP\*s to  
380 membrane-inserted  $\mu$ 1N and the subsequent penetration of reovirus cores. Within the  
381 *Reoviridae* family, bluetongue virus (BTV) outer-capsid protein VP5 penetrates late  
382 endosomal membranes enriched in phospholipid lysobisphosphatidic acid (LBPA),  
383 which is dependent on the anionic charge and membrane fluidic properties of LBPA  
384 (64). LBPA-enriched late endosomes also are required for efficient rotavirus entry (65).  
385 Our data demonstrating the importance of cholesterol homeostasis in reovirus entry,  
386 along with the role of LBPA in BTV and rotavirus entry, suggest that the lipid  
387 composition of late endosomes influences nonenveloped virus entry and illuminate a  
388 potential new target for antiviral therapy.

389 Our findings parallel those of a companion study indicating a function for WD  
390 repeat-containing protein 81 (WDR81) in reovirus entry (66). WDR81 was identified in a  
391 CRISPR/Cas9 cell-survival screen using mouse embryo fibroblasts and found to be  
392 required for a step in reovirus entry that follows ISVP formation. WDR81 is required for  
393 the maturation of late endosomes by modulating levels of phosphatidylinositol 3-

394 phosphate (67). These findings, coupled with our studies of NPC1, suggest that ISVPs  
395 formed in an altered endocytic compartment of cells lacking either WDR81 or NPC1  
396 cannot launch replication, whereas ISVPs adsorbed to the surface of such cells can.  
397 We think that alterations in cholesterol distribution might govern this difference in ISVP  
398 behavior.

399 Cholesterol accumulation due to NPC1 dysfunction also can lead to alterations in  
400 the distribution of host proteins, such as annexin A2 (ANXA2), which was identified in  
401 our siRNA screen, and annexin A6 (ANXA6) (68). ANXA2 and ANXA6 are  
402 multifunctional proteins involved in endosomal trafficking, segregation of membrane  
403 lipids, and membrane curvature regulation through membrane-cytoskeleton  
404 rearrangements (69). Disruption of NPC1 leads to increased concentrations of ANXA2  
405 and ANXA6 in late endosomes in response to cholesterol accumulation (70, 71). It is  
406 possible that cholesterol accumulation in cells lacking NPC1 similarly alters the  
407 distribution or function of WDR81. Thus, dysfunction of endosomal proteins in NPC1  
408 KO cells might alter potential interactions of  $\mu$ 1N or the reovirus core with specific lipid  
409 microdomains or proteins and inhibit core release.

410 Genetic screens are useful approaches to identify host factors required for viral  
411 replication and provide valuable information about virus-cell interactions (72, 73).  
412 However, genetic screens frequently yield long lists of potential candidates, many of  
413 which are false-positives. To increase the likelihood of identifying host factors required  
414 for reovirus replication, we compared gene lists obtained from independent genome-  
415 wide CRISPR/Cas9 and siRNA-based cell-survival screens. Only 28 genes in the  
416 CRISPR/Cas9 screens using strains T1L and T3D were identified in the siRNA screen  
417 using strain T3SA+, 19 of which are ribosomal genes (Fig. 1B, C). Of the nine non-  
418 ribosomal genes, several encode proteins required for reovirus entry, including those

419 involved in sialic acid biosynthesis and metabolism (*Nans* and *Neu*) (37, 38) and viral  
420 disassembly (*Ctsl*) (22).

421 Our findings indicate that NPC1, which was identified in both CRISPR/Cas9 and  
422 siRNA screens, is required for efficient release of reovirus cores into the cytoplasm by  
423 regulating cholesterol homeostasis. High-resolution studies showing the precise  
424 distribution of reovirus virions and cores within endosomes will be required to  
425 understand how NPC1 and cholesterol homeostasis regulate core release. These  
426 studies will allow us to answer the following new questions: Do cores interact with  
427 endosomal membranes in NPC1 KO cells? Does cholesterol impede interactions of  
428 cores with membranes? Are other lipids or proteins required for core release? Our  
429 ongoing work to answer these questions will clarify the functional elements of the  
430 reovirus entry pathway and lead to new approaches to block the entry of viruses that  
431 depend on tightly regulated cholesterol distribution in the endocytic pathway.

432 **MATERIALS AND METHODS**

433 **Cells and viruses**

434 HBMECs were cultured in growth medium (RPMI 1640 (Gibco) supplemented to  
435 contain 10% fetal bovine serum (FBS; VWR 97068-085), 10% Nu Serum (Corning), 1%  
436 MEM-vitamins (Corning), 1% sodium pyruvate (Gibco), 1% MEM non-essential amino  
437 acids (Gibco), 1% L-glutamine (Gibco), 1% penicillin/streptomycin (Gibco), and 0.1%  
438 amphotericin B (Sigma) or infection medium (growth medium containing 2% FBS). BV2  
439 mouse microglial cells were cultured in BV2 maintenance medium (DMEM  
440 supplemented to contain 10% FBS, 1% penicillin/streptomycin, 1% sodium pyruvate,  
441 and 1% sodium bicarbonate) or selection medium (maintenance media supplemented  
442 with 4 µg/ml blasticidin (Thermo Fisher) and 2.5 µg/ml puromycin (Sigma-Aldrich)).

443 HeLa cells were cultured in Dulbecco modified Eagle medium (Gibco) supplemented to  
444 contain 10% FBS, minimal essential medium nonessential amino acid solution (Gibco),  
445 0.11 mg/mL of sodium pyruvate (Gibco), and 1% penicillin/ streptomycin, and 0.1%  
446 amphotericin B (Sigma). Spinner-adapted L929 cells (originally obtained from the  
447 Bernard Fields laboratory; ATCC CCL-1) were grown in either suspension or  
448 monolayers in Joklik's modified Eagle's minimal essential medium (US Biological;  
449 M3867) supplemented to contain 5% FBS, 2 mM L-glutamine, 100 units/ml penicillin,  
450 100 µg/ml streptomycin, and 0.1% amphotericin B.

451 Reovirus strains T1L, T3D, T3SA+, and T1L M1-P208S, were prepared from  
452 laboratory stocks by plaque purification followed by 3 to 4 passages in L929 cells.  
453 T3SA+ contains nine genes from T1L and the S1 gene from T3C44-MA (36). T1L M1-  
454 P208S contains a point mutation in the M1 gene that causes viral factories to have a  
455 globular morphology similar to the morphology of factories formed by reovirus T3D (43)  
456 and can be readily scored for infection. Virions were purified from infected L929 cell

457 lysates using cesium chloride gradient centrifugation as described (74). Viral titers were  
458 determined by plaque assay using L929 cells (75) and expressed as plaque forming  
459 units per ml (PFU/ml). Reovirus particle concentration was estimated by spectral  
460 absorbance of purified virions at 260 nm (optical density at 260 nm [OD<sub>260</sub>] of 1 =  
461 2.1x10<sup>12</sup> particles/ml) (76).

462 Fluorescent reovirus particles were prepared by diluting 6 × 10<sup>12</sup> reovirus  
463 particles/ml in 50 mM sodium bicarbonate buffer and incubating with 20 μM Alexa  
464 Fluor™ 647 NHS Ester (Succinimidyl Ester) (Invitrogen, A37573) at room temperature  
465 (RT) for 90 min, protected from light (77). Labeled virions were dialyzed at 4°C  
466 overnight with 2-3 buffer exchanges to remove unreacted dye.

467 ISVPs were prepared by incubating 2 × 10<sup>12</sup> purified reovirus particles with 200  
468 μg/mL chymotrypsin (Sigma, C3142) at 37°C for 60 min (23). Digestion was terminated  
469 by the addition of PMSF to a final concentration of 2 mM. Virion-to-ISVP conversion  
470 was confirmed by SDS-PAGE and colloidal blue staining to assess the loss of σ3 and  
471 cleavage of μ1C to δ.

472

### 473 **Antibodies and dyes**

474 Primary antibodies used for indirect immunofluorescence include anti-CD63 (1:250)  
475 (Thermofisher, #10628D), reovirus-specific polyclonal rabbit antiserum (1:1000) (78),  
476 and T1L core-specific rabbit antiserum (1:250) provided by Max Nibert (79). Alexa Fluor  
477 conjugated secondary antibodies (Thermo Fisher, #A11034, #A11030) were used to  
478 visualize antigen. Nuclei were stained with 4',6-diamidino-2-phenylindole (DAPI,  
479 Invitrogen, D3571). Primary antibodies used for immunoblotting include reovirus-  
480 specific polyclonal rabbit antiserum, NPC1-specific polyclonal rabbit antiserum (Abcam,  
481 134113), and mouse GAPDH monoclonal antibody for protein loading controls (Sigma,

482 G8795). Anti-mouse IRDye680RD and anti-rabbit IRDye800CW (Licor) secondary  
483 antibodies were used.

484

485 **CRISPR Screen**

486 The screen was conducted and transduction validated as described (80). BV2 cells  
487 were transduced with pXPR\_101 lentivirus encoding Cas9 (Addgene; 52962) and  
488 propagated for 11 days with BV2 Maintenance Medium supplemented to contain  
489 blasticidin. These parental BV2 or BV2-Cas9 cells were transduced for 2 days with  
490 pXPR\_011 expressing eGFP (Addgene; 59702) and a short guide RNA (sgRNA)  
491 targeting eGFP at a multiplicity of infection (MOI) of less than 1 PFU/cell. Cells were  
492 selected for 5 days with BV2 selection medium. The frequency of eGFP-expressing  
493 cells was quantified by flow cytometry.

494 The murine Asiago sgRNA CRISPR library contains six independent genome-  
495 wide pools, in which each pool contains unique sgRNAs targeting 20,077 mouse genes.  
496 Four pools of the Asiago library were transduced into  $5 \times 10^7$  BV2 cells at an MOI of 0.2  
497 PFU/cell to establish four BV2 libraries. Two days post-transduction, cells were  
498 transferred to BV2 Selection Medium and propagated for 5 additional days. For each  
499 experimental condition,  $10^7$  BV2 library cells expressing Cas9 and sgRNAs were  
500 seeded in duplicate into T175 tissue culture flasks (Greiner Bio-One). Cells were  
501 inoculated with Opti-MEM supplemented to contain PBS (mock) or reovirus strains T1L  
502 or T3D at an MOI of 100 PFU/cell. Cells were incubated at RT for 1 h, followed by the  
503 addition of 20 mL of DMEM supplemented to contain 10% FBS, 1%  
504 penicillin/streptomycin, 1% sodium pyruvate, and 1% sodium bicarbonate. After 2 days  
505 post-inoculation (dpi) (mock) or 9 dpi (T1L or T3D conditions), cells were harvested and

506 genomic DNA (gDNA) was isolated from surviving cells using a QIAamp DNA Mini Kit  
507 (QIAGEN) according to the manufacturer's instructions.

508

509 **CRISPR screen sequencing and analysis**

510 Illumina sequencing and STARS analyses were conducted as described (81). The  
511 gDNA was aliquoted into a 96-well plate (Greiner Bio-One) with up to 10 µg gDNA in 50  
512 µL of total volume per well. A polymerase chain reaction (PCR) master mix containing  
513 ExTaq DNA polymerase (Clontech), ExTaq buffer (Clontech), dNTPs, P5 stagger  
514 primer, and water was prepared. PCR master mix (40 µL) and 10 µL of a barcoded  
515 primer were added to each well containing gDNA. Samples were amplified using the  
516 following protocol: 95°C for 1 min, followed by 28 cycles of 94°C for 50 s, 52.5°C for 30  
517 s, and 72°C for 30 s, and ending with a final 72°C extension for 10 min. PCR product  
518 was purified using Agencourt AMPure XP SPRI beads (Beckman Coulter) according to  
519 the manufacturer's instructions. Samples were sequenced using a HiSeq 2000  
520 (Illumina). Following deconvolution of the barcodes in the P7 primer, sgRNA sequences  
521 were mapped to a reference file of sgRNAs from the Asiago library. To account for the  
522 varying number of reads per condition, read counts per sgRNA were normalized to  $10^7$   
523 total reads per sample. Normalized values were then log-2 transformed. sgRNAs that  
524 were not detected were arbitrarily assigned a read count of 1. sgRNA frequencies were  
525 analyzed using STARS software to produce a rank ordered score for each gene. This  
526 score correlated with the sgRNA candidates that were above 10% of the total  
527 sequenced sgRNAs. Genes scoring above this threshold in either of the two  
528 independent subpools and in at least two of the four independent genome-wide pools  
529 were assigned a STAR score. In addition to the STAR score, screen results were

530 compared using false discovery rate (FDR) analyses to monitor gene-specific signal  
531 versus background noise. Statistical values of independent replicates were averaged.

532

533 **Whole genome siRNA screen and analysis**

534 The whole genome siRNA screen was conducted as described (35) using HeLa S3  
535 cells and the Dharmacon ON-TARGETplus® SMARTpool® human siRNA library  
536 (Thermo Scientific) and strain T3SA+.

537

538 **Production of NPC1 KO and KO+ cell lines**

539 HBMEC single-cell clones with ablation of the *NPC1* gene were engineered using  
540 CRISPR/Cas9-mediated gene editing as described (82) using an NPC1-specific gRNA  
541 (5' GGCCTTGTCAATTACTTGAGGGGG 3', targeting nucleotides 768-790 of the human  
542 *NPC1* mRNA). Single-cell clones were screened for the loss of NPC1 function by filipin  
543 III staining (82). Genotype of the selected NPC1 KO clones was confirmed by Sanger  
544 sequencing followed by amplification of the genomic DNA sequences flanking the  
545 gRNA target site using forward (5' TCATAAACACACCAAACTTGGAAATC 3') and  
546 reverse (5' TCCTGCGGCAGAGGTTTC 3') primers. Sequences of the NPC1 alleles  
547 were deconvoluted using CRISP-ID (83). To confirm the specificity of *Npc1* knockout,  
548 cells of a single clone were transduced with a retrovirus vector (pBabe-Puro)  
549 expressing human NPC1 as described (47).

550

551 **Indirect immunofluorescence staining**

552 Cells were fixed with 4% paraformaldehyde (PFA, Electron Microscopy Sciences,  
553 15712-s) in PBS<sup>-/-</sup> at RT for 20 min, washed three times with PBS<sup>-/-</sup>, and permeabilized  
554 and blocked with 0.1% Triton X-100 and 2% FBS in PBS<sup>-/-</sup> at RT for 20 min. Cells were

555 incubated sequentially with primary antibody, Alexa Fluor-conjugated secondary  
556 antibody, and DAPI diluted in PBS<sup>-/-</sup> containing 0.1% Triton X-100 and 2% FBS at RT  
557 for 30 to 60 min. For cholesterol labeling, fixed and permeabilized cells were incubated  
558 with 50 µg/ml filipin III (Sigma, SAE0088) diluted in PBS<sup>-/-</sup> for 30 min. Coverslips were  
559 mounted using Prolong-gold (Molecular Probes). Confocal images were captured using  
560 a Leica-SP8 laser scanning confocal microscope equipped with an HCX PL APO  
561 63X/1.4 N.A oil objective and processed using Fiji/ImageJ software.

562

### 563 **SDS-PAGE and Immunoblotting**

564 Cells harvested for protein extraction were lysed in Radioimmunoprecipitation Assay  
565 buffer (*RIPA buffer*; Thermo Fisher) supplemented with 1X protease inhibitors (Thermo  
566 Fisher). Protein concentration was quantified by Bradford assay (Bio-Rad) following the  
567 manufacturer's protocol. Samples for SDS-PAGE were diluted in 5X Laemmli sample  
568 buffer (Bio-Rad) containing 10% β-mercaptoethanol and incubated at 95°C for 10 min.  
569 Samples for detection of NPC1 were incubated at 70°C for 10 min to prevent  
570 aggregation. Equal amounts of protein were electrophoresed in 10% or 4-20% Mini-  
571 Protean TGX gels (Bio-Rad). Following electrophoresis, proteins were transferred to  
572 nitrocellulose membranes (Bio-Rad) for immunoblotting. Nitrocellulose membranes  
573 were incubated with 5% nonfat milk in TBS (50 mM Tris-HCl, pH 7.6; 150 mM NaCl)  
574 with 0.1% Tween 20 (TBS-T) and sequentially incubated with primary and secondary  
575 antibodies diluted in TBS-T at RT for 1 h. Immunoblot images were captured using an  
576 Odyssey CLx imaging system (Li-Cor) and protein bands were quantified using the  
577 Image Studio Lite software. Protein expression levels were normalized to GAPDH  
578 loading controls.

579

580 **Quantification of reovirus infectivity**

581 In experiments comparing infectivity of reovirus in KO, KO+, and WT HBMECs, cells  
582 were adsorbed with 10,000 reovirus virions or 100 ISVPs diluted in Opti-MEM  
583 (Invitrogen) at 37°C for 1 h. Following adsorption, the inoculum was removed, and cells  
584 were incubated in infection medium for 18 h before fixing in ice-cold methanol. In  
585 experiments comparing reovirus infectivity in the presence or absence of H $\beta$ CD, cells  
586 were treated with 1 mM H $\beta$ CD or PBS for 24 h prior to adsorption with reovirus.  
587 Following adsorption, fresh 1 mM H $\beta$ CD was added to the medium for 18 h before fixing  
588 in ice-cold methanol. Fixed cells were washed with PBS $^{-/-}$ , blocked with 1% bovine  
589 serum albumin (BSA), and incubated sequentially with reovirus-specific polyclonal  
590 rabbit antiserum, Alexa Fluor 488-conjugated anti-rabbit antibody, and DAPI in PBS $^{-/-}$   
591 containing 0.5% Triton X-100. Cells were imaged using a Lionheart FX automated  
592 imager (BioTek) equipped with a 20X air objective, taking four fields-of-view from  
593 duplicate samples. Images were processed and signals quantified using Gen5+  
594 software (BioTek).

595

596 **Viral binding**

597 KO, KO+, and WT HBMECs were detached from tissue-culture plates using  
598 CellStripper dissociation reagent (Corning), quenched with HBMEC medium, and  
599 washed with PBS $^{-/-}$ . Cells were resuspended in PBS $^{-/-}$  at 10<sup>6</sup> cells/ml and adsorbed with  
600 10,000 Alexa Fluor 647-labeled reovirus virions/cell at 4°C for 1 h with agitation. After  
601 binding, cells were washed twice with PBS $^{-/-}$  and fixed with 1% paraformaldehyde (PFA)  
602 supplemented with propidium iodide to determine cell viability. Cells were analyzed  
603 using an LSRII flow cytometer (BD Bioscience). Results were quantified using FlowJo  
604 V10 software.

605

606 **Live microscopy of reovirus internalization**

607 KO, KO+, and WT HBMECs were plated on glass-bottom p35 plates and adsorbed with  
608 10,000 Alexa 647-labeled reovirus virions/cell at 4°C for 45 min to synchronize  
609 infection. The inoculum was removed and replaced with fresh Opti-MEM without  
610 phenol-red medium supplemented with 2% FBS. Reovirus transport was imaged using  
611 a Leica DMI6000B fluorescence microscope with an HCX PL APO 63X/1.30 Gly  
612 objective. Fluorescence and brightfield images were collected from 0 to 36 min post  
613 adsorption every ~ 25 sec.

614

615 **Tracking of reovirus transport**

616 Automated tracking of fluorescent reovirus particles in time-lapse images was  
617 conducted using Icy bioimage analysis software. Regions of interest (ROI)  
618 corresponding to the cell periphery were selected for tracking analysis using the Spot  
619 Detector plugin (84). The scale of the object (reovirus virions) to be analyzed was set at  
620 a size of ~7 pixels per spot, and the threshold sensitivity was set at 100. Parameters  
621 describing transport dynamics were considered as both diffusive and directed for  
622 running tracking analysis. Results are presented in colored time-dependent tracks.

623

624 **Quantification of reovirus cores**

625 KO, KO+, and WT HBMECs were adsorbed with 10,000 Alexa Fluor 647-labeled  
626 reovirus virions at 37°C for 45 min. The inoculum was removed, and the cells were  
627 incubated in infection medium containing 100 µg/ml of cycloheximide for 8 h. After  
628 fixation, cells were permeabilized and stained with T1L core-specific rabbit polyclonal  
629 serum and anti-CD63 antibody. Confocal images were captured using a Leica-SP8

630 laser scanning confocal microscope equipped with an HCX PL APO 63X/1.4 N.A oil  
631 objective and processed using Fiji/ImageJ software. Colocalization of fluorescent  
632 reovirus virions (cyan puncta), reovirus cores (green puncta), and late endosomes (red  
633 puncta) was analyzed to differentiate infecting virions from cores released into the  
634 cytoplasm.

635

### 636 **RNA extraction and purification**

637 Cells were lysed using TRIzol reagent (Invitrogen). RNA was extracted with chloroform  
638 and purified using a PureLink RNA minikit (Invitrogen) with DNase treatment according  
639 to the manufacturer's instructions.

640

### 641 **S4 quantitative RT-PCR**

642 Total S4 RNA was quantified using qScript XLT one-step RT-qPCR ToughMix, Low  
643 ROX (Quanta Bioscience) and T3D\_S4\_qPCR primers (Forward:  
644 GAAGCATTGCCTCACCATAG, Reverse: GATCTGTCCAATTGAGTGTATTG)  
645 according to the manufacturer's instructions. The following RT-qPCR cycling protocol  
646 was used: cDNA synthesis (50°C for 10 min), initial denaturation (95°C for 1 min), and  
647 40 PCR cycles (95°C for 10 s followed by a data collection step at 60°C for 1 min). S4  
648 cDNA was detected using a fluorogenic probe (5'-FAM [fluorescent fluorescein]-  
649 AGCGCGCAAGAGGGATGGGA-BHQ [black hole quencher]-1-3'; Biosearch  
650 Technologies).

651

### 652 **Statistical analysis**

653 All data were analyzed using Graphpad Prism 8. Figure legends specify the number of  
654 experimental repeats and the statistical test applied for each analysis. Differences were  
655 considered statistically significant when *P* values were less than 0.05.

656 **Acknowledgements**

657 We thank members of the Dermody and Risco laboratories for many useful discussions  
658 and Dr. Pranav Danthi for review of the manuscript and sharing data from his laboratory  
659 prior to publication. We thank Dr. Martin Sachse for expert advice and review of the  
660 manuscript and Drs. Sylvia Gutiérrez-Erlundsson and Ana Oña for assistance with  
661 confocal microscopy. We are grateful to the UPMC Children's Hospital of Pittsburgh  
662 Rangos Research Center Cell Imaging Core Laboratory for assistance with microscopy.

663 This work was supported in part by Public Health Service award R01 AI032539  
664 (C.R. and T.S.D.) and the Heinz Endowments (T.S.D.) and grants BIO2015-68758-R  
665 and RTI2018-094445-B-100 from the Ministry of Science and Innovation of Spain  
666 (C.R.).

667

668 **Competing interests**

669 The authors have declared that no competing interests exist.

670

671 **Author contributions**

672 **Conceived and designed experiments:** POG, GT, CR, and TSD. **Conducted**  
673 **experiments:** POG, GT, RKJ, BAM, RCO, and CBW. **Analyzed data:** POG and GT.  
674 **Contributed reagents/materials/analysis tools:** RKJ, RCO, CBW, and KC. **Wrote**  
675 **original draft:** POG, GT, and TSD. **Reviewed and edited paper:** POG, GT, RKJ, RT,  
676 IF, BAM, RCO, CBW, PAB, JS, KC, CR, and TSD.

677 **REFERENCES**

678 1. Mercer J, Helenius A. Virus entry by macropinocytosis. *Nat Cell Biol.* 2009;11(5):510-20.

680 2. Mercer J, Schelhaas M, Helenius A. Virus entry by endocytosis. *Annu Rev*  
681 *Biochem.* 2010;79:803-33.

682 3. Yamauchi Y, Helenius A. Virus entry at a glance. *J Cell Sci.* 2013;126(Pt  
683 6):1289-95.

684 4. Smith AE, Helenius A. How viruses enter animal cells. *Science.* 2004;304(5668):237-42.

686 5. Tsai B. Penetration of nonenveloped viruses into the cytoplasm. *Annu Rev Cell*  
687 *Develop Biol.* 2007;23:23-43.

688 6. Staring J, Raaben M, Brummelkamp TR. Viral escape from endosomes and host  
689 detection at a glance. *J Cell Sci.* 2018;131(15).

690 7. Harrison SC. Viral membrane fusion. *Virology.* 2015;479-480:498-507.

691 8. White JM, Whittaker GR. Fusion of enveloped viruses in endosomes. *Traffic.*  
692 2016;17(6):593-614.

693 9. Sieczkarski SB, Whittaker GR. Viral entry. *Curr Top Microbiol Immunol.*  
694 2005;285:1-23.

695 10. Plemper RK. Cell entry of enveloped viruses. *Curr Opin Virol.* 2011;1(2):92-100.

696 11. Stewart PL, Dermody TS, Nemerow GR. Structural basis of nonenveloped virus  
697 cell entry. *Adv Protein Chem.* 2003;64:455-91.

698 12. Kumar CS, Dey D, Ghosh S, Banerjee M. Breach: Host membrane penetration  
699 and entry by nonenveloped viruses. *Trends Microbiol.* 2018;26(6):525-37.

700 13. Banerjee M, Johnson JE. Activation, exposure and penetration of virally  
701 encoded, membrane-active polypeptides during non-enveloped virus entry. *Curr Protein*  
702 *Pept Sci.* 2008;9(1):16-27.

703 14. Bouziat R, Hinterleitner R, Brown JJ, Stencel-Baerenwald JE, Ikizler M, Mayassi  
704 T, et al. Reovirus infection triggers inflammatory responses to dietary antigens and  
705 development of celiac disease. *Science.* 2017;356(6333):44-50.

706 15. Dryden KA, Wang G, Yeager M, Nibert ML, Coombs KM, Furlong DB, et al. Early  
707 steps in reovirus infection are associated with dramatic changes in supramolecular  
708 structure and protein conformation: analysis of virions and subviral particles by  
709 cryoelectron microscopy and image reconstruction. *J Cell Biol.* 1993;122(5):1023-41.

710 16. Zhang X, Ji Y, Zhang L, Harrison SC, Marinescu DC, Nibert ML, et al. Features  
711 of reovirus outer capsid protein m1 revealed by electron cryomicroscopy and image  
712 reconstruction of the virion at 7.0 Å resolution. *Structure.* 2005;13(10):1545-57.

713 17. Dermody TS, Parker JS, Sherry B. Orthoreoviruses. In: Knipe DM, Howley PM,  
714 editors. *Fields Virology*. 2. 6th ed. Philadelphia: Lippincott Williams & Wilkins; 2013. p.  
715 1304-46.

716 18. Gummersheimer SL, Snyder AJ, Danthi P. Control of capsid transformations  
717 during reovirus entry. *Viruses*. 2021;13(2):153.

718 19. Roth AN, Aravamudhan P, Fernández de Castro I, Tenorio R, Risco C, Dermody  
719 TS. Ins and outs of reovirus: vesicular trafficking in viral entry and egress. *Trends*  
720 *Microbiol*. 2021;29(4):363-75.

721 20. Borsa J, Sargent MD, Lievaart PA, Coppers TP. Reovirus: evidence for a second  
722 step in the intracellular uncoating and transcriptase activation process. *Virology*.  
723 1981;111(1):191-200.

724 21. Sturzenbecker LJ, Nibert ML, Furlong DB, Fields BN. Intracellular digestion of  
725 reovirus particles requires a low pH and is an essential step in the viral infectious cycle.  
726 *J Virol* 1987;61(8):2351-61.

727 22. Ebert DH, Deussing J, Peters C, Dermody TS. Cathepsin L and cathepsin B  
728 mediate reovirus disassembly in murine fibroblast cells. *J Biol Chem*.  
729 2002;277(27):24609-17.

730 23. Baer GS, Dermody TS. Mutations in reovirus outer-capsid protein s3 selected  
731 during persistent infections of L cells confer resistance to protease inhibitor E64. *J Virol*.  
732 1997;71:4921-8.

733 24. Silverstein SC, Astell C, Levin DH, Schonberg M, Acs G. The mechanism of  
734 reovirus uncoating and gene activation in vivo. *Virology*. 1972;47(3):797-806.

735 25. Snyder AJ, Danthi P. Lipid membranes facilitate conformational changes  
736 required for reovirus cell entry. *J Virol*. 2015;90(5):2628-38.

737 26. Snyder AJ, Danthi P. Lipids cooperate with the reovirus membrane penetration  
738 peptide to facilitate particle uncoating. *J Biol Chem*. 2016;291(52):26773-85.

739 27. Odegard AL, Chandran K, Zhang X, Parker JS, Baker TS, Nibert ML. Putative  
740 autocleavage of outer capsid protein m1, allowing release of myristoylated peptide m1N  
741 during particle uncoating, is critical for cell entry by reovirus. *J Virol*. 2004;78(16):8732-  
742 45.

743 28. Agosto MA, Ivanovic T, Nibert ML. Mammalian reovirus, a nonfusogenic  
744 nonenveloped virus, forms size-selective pores in a model membrane. *Proc Natl Acad  
745 Sci U S A*. 2006;103(44):16496-501.

746 29. Ivanovic T, Agosto MA, Zhang L, Chandran K, Harrison SC, Nibert ML. Peptides  
747 released from reovirus outer capsid form membrane pores that recruit virus particles.  
748 *EMBO J*. 2008;27(8):1289-98.

749 30. Chandran K, Farsetta DL, Nibert ML. Strategy for nonenveloped virus entry: a  
750 hydrophobic conformer of the reovirus membrane penetration protein m1 mediates  
751 membrane disruption. *J Virol*. 2002;76(19):9920-33.

752 31. Zhang L, Agosto MA, Ivanovic T, King DS, Nibert ML, Harrison SC.  
753 Requirements for the formation of membrane pores by the reovirus myristoylated  
754 micro1N peptide. *J Virol.* 2009;83(14):7004-14.

755 32. Carstea ED, Morris JA, Coleman KG, Loftus SK, Zhang D, Cummings C, et al.  
756 Niemann-Pick C1 disease gene: homology to mediators of cholesterol homeostasis.  
757 *Science.* 1997;277(5323):228-31.

758 33. Ioannou YA. The structure and function of the Niemann-Pick C1 protein. *Mol  
759 Genet Metab.* 2000;71(1-2):175-81.

760 34. Kwon HJ, Abi-Mosleh L, Wang ML, Deisenhofer J, Goldstein JL, Brown MS, et  
761 al. Structure of N-terminal domain of NPC1 reveals distinct subdomains for binding and  
762 transfer of cholesterol. *Cell.* 2009;137(7):1213-24.

763 35. Konopka-Anstadt JL, Mainou BA, Sutherland DM, Sekine Y, Strittmatter SM,  
764 Dermody TS. The Nogo receptor NgR1 mediates infection by mammalian reovirus. *Cell  
765 Host Microbe.* 2014;15(6):681-91.

766 36. Barton ES, Connolly JL, Forrest JC, Chappell JD, Dermody TS. Utilization of  
767 sialic acid as a coreceptor enhances reovirus attachment by multistep adhesion  
768 strengthening. *J Biol Chem.* 2001;276(3):2200-11.

769 37. Urbanek K, Sutherland DM, Orchard RC, Wilen CB, Knowlton JJ, Aravamudhan  
770 P, et al. Cytidine monophosphate N-acetylneurameric acid synthetase and solute carrier  
771 family 35 member A1 are required for reovirus binding and infection. *J Virol.* 2020;95(2).

772 38. Gentsch JR, Pacitti AF. Effect of neuraminidase treatment of cells and effect of  
773 soluble glycoproteins on type 3 reovirus attachment to murine L cells. *J Virol.*  
774 1985;56(2):356-64.

775 39. Avula K, Singh B, Kumar PV, Syed GH. Role of lipid transfer proteins (LTPs) in  
776 the viral life cycle. *Front Microbiol.* 2021;12:673509.

777 40. Lai CM, Mainou BA, Kim KS, Dermody TS. Directional release of reovirus from  
778 the apical surface of polarized endothelial cells. *mBio.* 2013;4(2):e00049-13.

779 41. Fu J, Li L, Huo D, Zhi S, Yang R, Yang B, et al. Astrocyte-derived TGF $\beta$ 1  
780 facilitates blood-brain barrier function via non-canonical hedgehog signaling in brain  
781 microvascular endothelial cells. *Brain Sci.* 2021;11(1).

782 42. Borsa J, Copps TP, Sargent MD, Long DG, Chapman JD. New intermediate  
783 subviral particles in the in vitro uncoating of reovirus virions by chymotrypsin. *J Virol.*  
784 1973;11(4):552-64.

785 43. Parker JS, Broering TJ, Kim J, Higgins DE, Nibert ML. Reovirus core protein m2  
786 determines the filamentous morphology of viral inclusion bodies by interacting with and  
787 stabilizing microtubules. *J Virol.* 2002;76(9):4483-96.

788 44. Aravamudhan P, Raghunathan K, Konopka-Anstadt J, Pathak A, Sutherland DM,  
789 Carter BD, et al. Reovirus uses macropinocytosis-mediated entry and fast axonal  
790 transport to infect neurons. *PLoS Pathog.* 2020;16(2):e1008380.

791 45. Elrick MJ, Yu T, Chung C, Lieberman AP. Impaired proteolysis underlies  
792 autophagic dysfunction in Niemann-Pick type C disease. *Hum Mol Genet*.  
793 2012;21(22):4876-87.

794 46. Carette JE, Raaben M, Wong AC, Herbert AS, Obernosterer G, Mulherkar N, et  
795 al. Ebola virus entry requires the cholesterol transporter Niemann-Pick C1. *Nature*.  
796 2011;477(7364):340-3.

797 47. Miller EH, Obernosterer G, Raaben M, Herbert AS, Deffieu MS, Krishnan A, et al.  
798 Ebola virus entry requires the host-programmed recognition of an intracellular receptor.  
799 *EMBO J*. 2012;31(8):1947-60.

800 48. Rosenbaum AI, Zhang G, Warren JD, Maxfield FR. Endocytosis of beta-  
801 cyclodextrins is responsible for cholesterol reduction in Niemann-Pick type C mutant  
802 cells. *Proc Natl Acad Sci U S A*. 2010;107(12):5477-82.

803 49. Peake KB, Vance JE. Normalization of cholesterol homeostasis by 2-  
804 hydroxypropyl- $\beta$ -cyclodextrin in neurons and glia from Niemann-Pick C1 (NPC1)-  
805 deficient mice. *J Biol Chem*. 2012;287(12):9290-8.

806 50. Liu B, Turley SD, Burns DK, Miller AM, Repa JJ, Dietschy JM. Reversal of  
807 defective lysosomal transport in NPC disease ameliorates liver dysfunction and  
808 neurodegeneration in the npc1-/- mouse. *Proc Natl Acad Sci U S A*. 2009;106(7):2377-  
809 82.

810 51. Ory DS, Ottinger EA, Farhat NY, King KA, Jiang X, Weissfeld L, et al. Intrathecal  
811 2-hydroxypropyl- $\beta$ -cyclodextrin decreases neurological disease progression in  
812 Niemann-Pick disease, type C1: a non-randomised, open-label, phase 1-2 trial. *Lancet*.  
813 2017;390(10104):1758-68.

814 52. Poh MK, Shui G, Xie X, Shi PY, Wenk MR, Gu F. U18666A, an intra-cellular  
815 cholesterol transport inhibitor, inhibits dengue virus entry and replication. *Antiviral Res*.  
816 2012;93(1):191-8.

817 53. Cuesta-Geijo M, Chiappi M, Galindo I, Barrado-Gil L, Muñoz-Moreno R,  
818 Carrascosa JL, et al. Cholesterol flux is required for endosomal progression of African  
819 swine fever virions during the initial establishment of infection. *J Virol*. 2016;90(3):1534-  
820 43.

821 54. Elgner F, Ren H, Medvedev R, Ploen D, Himmelsbach K, Boller K, et al. The  
822 intracellular cholesterol transport inhibitor U18666A inhibits the exosome-dependent  
823 release of mature hepatitis C virus. *J Virol*. 2016;90(24):11181-96.

824 55. Yin X, Ambadekar C, Lu Y, Feng Z. Distinct entry mechanisms for  
825 nonenveloped and quasi-enveloped hepatitis E viruses. *J Virol*. 2016;90(8):4232-42.

826 56. Rivera-Serrano EE, González-López O, Das A, Lemon SM. Cellular entry and  
827 uncoating of naked and quasi-enveloped human hepatoviruses. *eLife*. 2019;8.

828 57. Sobo K, Le Blanc I, Luyet PP, Fivaz M, Ferguson C, Parton RG, et al. Late  
829 endosomal cholesterol accumulation leads to impaired intra-endosomal trafficking. *PLoS  
830 one*. 2007;2(9):e851.

831 58. Vanier MT. Niemann-Pick disease type C. *Orphanet J Rare Dis*. 2010;5:16.

832 59. Koller D, Lohner K. The role of spontaneous lipid curvature in the interaction of  
833 interfacially active peptides with membranes. *Biochim Biophys Acta*.  
834 2014;1838(9):2250-9.

835 60. Maier O, Galan DL, Wodrich H, Wiethoff CM. An N-terminal domain of  
836 adenovirus protein VI fragments membranes by inducing positive membrane curvature.  
837 *Virology*. 2010;402(1):11-9.

838 61. Guo X, Steinkühler J, Marin M, Li X, Lu W, Dimova R, et al. Interferon-induced  
839 transmembrane protein 3 blocks fusion of diverse enveloped viruses by altering  
840 mechanical properties of cell membranes. *ACS Nano*. 2021;15(5):8155-70.

841 62. Anafu AA, Bowen CH, Chin CR, Brass AL, Holm GH. Interferon-inducible  
842 transmembrane protein 3 (IFITM3) restricts reovirus cell entry. *J Biol Chem*.  
843 2013;288(24):17261-71.

844 63. Moyer CL, Wiethoff CM, Maier O, Smith JG, Nemerow GR. Functional genetic  
845 and biophysical analyses of membrane disruption by human adenovirus. *J Virol*.  
846 2011;85(6):2631-41.

847 64. Patel A, Mohl BP, Roy P. Entry of Bluetongue virus capsid requires the late  
848 endosome-specific lipid lysobisphosphatidic acid. *J Biol Chem*. 2016;291(23):12408-19.

849 65. Silva-Ayala D, López T, Gutiérrez M, Perrimon N, López S, Arias CF. Genome-  
850 wide RNAi screen reveals a role for the ESCRT complex in rotavirus cell entry. *Proc  
851 Natl Acad Sci U S A*. 2013;110(25):10270-5.

852 66. Snyder A, Abad A, Danthi, P. A CRISPR-Cas9 screen reveals a role for WD  
853 repeat-containing protein (WDR81) in the entry of late penetrating viruses. bioRxiv  
854 preprint, doi:<https://biorxiv.org/cgi/content/short/2021.09.26.461887v1>, 2021.

855 67. Liu K, Jian Y, Sun X, Yang C, Gao Z, Zhang Z, et al. Negative regulation of  
856 phosphatidylinositol 3-phosphate levels in early-to-late endosome conversion. *J Cell  
857 Biol*. 2016;212(2):181-98.

858 68. Wheeler S, Schmid R, Sillence DJ. Lipid-protein interactions in Niemann-Pick  
859 type C Disease: Insights from molecular modeling. *Int J Mol Sci*. 2019;20(3).

860 69. Rentero C, Blanco-Munoz P, Meneses-Salas E, Grewal T, Enrich C. Annexins-  
861 coordinators of cholesterol homeostasis in endocytic pathways. *Int J Mol Sci*.  
862 2018;19(5):E1444.

863 70. de Diego I, Schwartz F, Siegfried H, Dauterstedt P, Heeren J, Beisiegel U, et al.  
864 Cholesterol modulates the membrane binding and intracellular distribution of annexin 6.  
865 *J Biol Chem*. 2002;277(35):32187-94.

866 71. Mayran N, Parton RG, Gruenberg J. Annexin II regulates multivesicular  
867 endosome biogenesis in the degradation pathway of animal cells. *EMBO J*.  
868 2003;22(13):3242-53.

869 72. Hirsch AJ. The use of RNAi-based screens to identify host proteins involved in  
870 viral replication. *Future Microbiol*. 2010;5(2):303-11.

871 73. Puschnik AS, Majzoub K, Ooi YS, Carette JE. A CRISPR toolbox to study virus-  
872 host interactions. *Nat Rev Microbiol.* 2017;15(6):351-64.

873 74. Furlong DB, Nibert ML, Fields BN. Sigma 1 protein of mammalian reoviruses  
874 extends from the surfaces of viral particles. *J Virol.* 1988;62(1):246-56.

875 75. Virgin HW, Bassel-Duby R, Fields BN, Tyler KL. Antibody protects against lethal  
876 infection with the neurally spreading reovirus type 3 (Dearing). *J Virol.*  
877 1988;62(12):4594-604.

878 76. Smith RE, Zweerink HJ, Joklik WK. Polypeptide components of virions, top  
879 component and cores of reovirus type 3. *Virology.* 1969;39(4):791-810.

880 77. Fecek RJ, Busch R, Lin H, Pal K, Cunningham CA, Cuff CF. Production of Alexa  
881 Fluor 488-labeled reovirus and characterization of target cell binding, competence, and  
882 immunogenicity of labeled virions. *J Immunol Methods.* 2006;314(1-2):30-7.

883 78. Wetzel JD, Chappell JD, Fogo AB, Dermody TS. Efficiency of viral entry  
884 determines the capacity of murine erythroleukemia cells to support persistent infections  
885 by mammalian reoviruses. *J Virol.* 1997;71(1):299-306.

886 79. Chandran K, Walker SB, Chen Y, Contreras CM, Schiff LA, Baker TS, et al. In  
887 vitro recoating of reovirus cores with baculovirus-expressed outer-capsid proteins  $\mu 1$   
888 and  $\sigma 3$ . *J Virol.* 1999;73(5):3941-50.

889 80. Orchard RC, Wilen CB, Doench JG, Baldridge MT, McCune BT, Lee YC, et al.  
890 Discovery of a proteinaceous cellular receptor for a norovirus. *Science.*  
891 2016;353(6302):933-6.

892 81. Doench JG, Fusi N, Sullender M, Hegde M, Vaimberg EW, Donovan KF, et al.  
893 Optimized sgRNA design to maximize activity and minimize off-target effects of  
894 CRISPR-Cas9. *Nat Biotechnol.* 2016;34(2):184-91.

895 82. Spence JS, Krause TB, Mittler E, Jangra RK, Chandran K. Direct visualization of  
896 ebola virus fusion triggering in the endocytic pathway. *mBio.* 2016;7(1):e01857-15.

897 83. Dehairs J, Talebi A, Cherifi Y, Swinnen JV. CRISP-ID: decoding CRISPR  
898 mediated indels by Sanger sequencing. *Sci Rep.* 2016;6:28973.

899 84. Olivio-Marin JC. Extraction of spots in biological images using multi-scale  
900 products. *Pattern Recognition.* 2002;35(9):1989-96.

901 **FIGURE LEGENDS**

902

903 **Fig. 1. CRISPR and siRNA screens identify NPC1 as a cellular factor required for**  
904 **reovirus infection.** (A) The top 20 candidates from the CRISPR screen using reovirus  
905 strains T1L and T3D are ranked by their STAR scores. Heat map indicates STAR  
906 values. (B) Genes from the siRNA screen using reovirus strain T3SA+ common to the  
907 CRISPR screen using T1L and T3D, excluding ribosomal genes. Heat map indicates z-  
908 score values. (C) Venn diagram of genes from the CRISPR screens using T1L and T3D  
909 and the siRNA screen using T3SA+. (D) Molecular function pathways using Gene  
910 Ontology to analyze genes from the CRISPR screen common to T1L and T3D. (E)  
911 KEGG pathways identified for the CRISPR screen using T1L (red) and T3D (blue) and  
912 siRNA screen using T3SA+ (light blue).

913

914 **Fig. 2. Viral infectivity and titers following adsorption by reovirus virions and**  
915 **ISVPs.** (A, B) WT, KO, and KO+ HBMECs were adsorbed with reovirus (A) virions or  
916 (B) ISVPs at MOIs of 10,000 or 100 particles/cell, respectively, and fixed at 18 h post-  
917 adsorption. The percentage of infected cells was determined by enumerating reovirus-  
918 infected cells following immunostaining with a reovirus-specific antiserum. (C-F) WT,  
919 KO, and KO+ cells were adsorbed with reovirus (C, E) virions at an MOI of 1 PFU/cell  
920 or (D, F) ISVPs at an MOI of 5 particles/cell. Viral titers in cell-culture supernatants and  
921 lysates were determined by plaque assay at 0, 24, and 48 h post-adsorption. The  
922 results are presented as the mean of three independent experiments. Error bars  
923 indicated standard deviation. \*,  $P < 0.05$ ; \*\*,  $P < 0.01$ ; \*\*\*,  $P < 0.001$ ; \*\*\*\*,  $P < 0.0001$ ,  
924 as determined by t-test.

925

926 **Fig. 3. Binding, internalization, and uncoating are not disrupted by cholesterol**  
927 **accumulation in NPC1 KO HBMECs.** (A) WT, KO, and KO+ HBMECs were adsorbed  
928 with Alexa 647 labeled-reovirus virions at an MOI of 10,000 particles/cell at 4°C for 1 h,  
929 fixed with 1% PFA, and analyzed for virus binding using flow cytometry. The results are  
930 presented as mean virus binding as determined by mean fluorescence intensity (MFI) of  
931 three independent experiments. Error bars indicated standard deviation. (B) WT, KO,  
932 and KO+ HBMECs were adsorbed with Alexa 647 labeled-reovirus virions at an MOI of  
933 10,000 particles/cell at 4°C for 45 min and imaged using high magnification live-cell  
934 imaging, with images captured every ~ 25 seconds. Representative micrographs from  
935 videos at the indicated intervals are shown. Scale bars, 10  $\mu$ m. (C) WT, KO, and KO+  
936 HBMECs were adsorbed with reovirus virions at an MOI of 10,000 particles/cell at 4°C  
937 for 1 h and lysed at the intervals post-adsorption shown. Cell lysates were subjected to  
938 electrophoresis and immunoblotting using a reovirus-specific polyclonal rabbit  
939 antiserum. The results are presented as the mean ratio of the  $\delta$  and  $\mu 1C$  bands from  
940 three independent experiments. Error bars indicate standard deviation. Differences are  
941 not significant, as determined by two-tailed unpaired t-test.

942

943 **Fig. 4. Cytosolic entry of reovirus cores.** (A) WT, KO, and KO+ HBMECs were  
944 adsorbed with Alexa 647 labeled-reovirus virions at an MOI of 10,000 particles/cell at  
945 37°C for 45 min and fixed with 4% PFA at 8 h post-adsorption. Cells were stained with  
946 DAPI, a CD-63-specific antibody to label endosomes, and an antiserum specific for  
947 reovirus cores, and imaged using confocal microscopy. Representative confocal  
948 micrographs are shown. (B) Colocalization of reovirus, cores, and endosomes was  
949 analyzed using the JaCoP plugin function from ImageJ. The results are presented as  
950 the mean colocalization (quantified by Manders coefficient) of ~ 50 cells from three

951 independent experiments. Error bars indicate standard deviation. \*\*,  $P < 0.01$ ; \*\*\*,  $P <$   
952 0.001, as determined by two-tailed unpaired t-test.

953

954 **Fig. 5. Synthesis of nascent RNA is reduced in NPC1 KO HBMECs.** WT, KO, and  
955 KO+ HBMECs were adsorbed with reovirus virions at an MOI of 1 PFU/cell at 37°C for  
956 1 h, lysed at the intervals post-adsorption shown, and assayed for positive-sense  
957 reovirus s4 RNA by RT-qPCR. The results are presented as the mean number of  
958 copies of reovirus s4 RNA by qPCR from two independent experiments. Error bars  
959 indicate standard errors of the mean. \*\*,  $P < 0.01$ ; \*\*\*,  $P < 0.001$ , as determined by t-  
960 test.

961

962 **Fig. 6. H $\beta$ CD treatment restores reovirus infection of NPC1 KO HBMECs.** WT, KO,  
963 and KO+ HBMECs were pretreated with 1 mM H $\beta$ CD or PBS for 24 h, adsorbed with  
964 reovirus virions or ISVPs at MOIs of 10,000 or 100 particles/cell, respectively, and fixed  
965 at 18 h post-adsorption. The percentage of infected cells was determined by  
966 enumerating reovirus-infected cells following immunostaining with a reovirus-specific  
967 antiserum. The results are presented as the mean of three independent experiments.  
968 Error bars indicated standard deviation. \*\*\*,  $P < 0.001$  as determined by two-tailed  
969 unpaired t-test.

970

971 **SUPPLEMENTAL MATERIALS**

972 **FIGURES AND MOVIES**

973

974 **Fig. S1. Effect on cholesterol distribution by disruption of NPC1 expression.** (A,  
975 B) Lysates of WT, KO, and KO+ HBMECs were subjected to electrophoresis and

976 immunoblotting using an NPC1 antiserum. GAPDH was used as loading control. A  
977 representative immunoblot is shown. The results are presented as the mean of two  
978 independent experiments. Error bars indicate standard deviation. Statistical analysis  
979 was done by two-tailed unpaired t-test. (C) WT, KO, and KO+ HBMECs were stained  
980 with filipin III to detect cholesterol distribution. Representative images are shown. Scale  
981 bars, 10  $\mu$ m. (D) WT, KO, and KO+ HBMECs were stained with filipin III and an anti-  
982 CD63 antibody to detect the subcellular localization of cholesterol. Representative  
983 images are shown. Scale bars, 10  $\mu$ m.

984

985 **Fig. S2. Viral infectivity following adsorption by T1L, T3D, and T3SA+ virions.** (A,  
986 B) WT, KO, and KO+ HBMECs were adsorbed with reovirus virions at MOIs of 10,000  
987 particles/cell, and fixed at 18 h post-adsorption. The percentage of infected cells was  
988 determined by enumerating reovirus-infected cells following immunostaining with a  
989 reovirus-specific antiserum. Error bars indicated standard deviation. \*\*,  $P < 0.01$ ; \*\*\*,  $P$   
990  $< 0.001$ , as determined by 2-way ANOVA, Tukey's multiple comparisons test.

991

992 **Fig. S3. H $\beta$ CD treatment restores cholesterol efflux in KO cells.** (A) WT, KO, and  
993 KO+ HBMECs were treated with H $\beta$ CD at the concentrations shown for 48 h and  
994 assessed for viability using the Presto blue cell viability reagent. The results are  
995 presented as the mean cell viability of three independent experiments. Error bars  
996 indicated standard deviation. \*\*,  $P < 0.01$ ; \*\*\*,  $P < 0.001$ ; \*\*\*\*,  $P < 0.0001$ , as  
997 determined by two-way ANOVA. (B, C) Cells were treated with 1 mM H $\beta$ CD or PBS  
998 (mock) for 48 h, fixed with 4% PFA, stained with filipin III, and imaged using confocal  
999 microscopy. (B) The results are presented as the mean filipin III staining (quantified by  
1000 MFI) of  $\sim$  50 cells from three independent experiments. Error bars indicate the minimum

1001 and the maximum values. \*,  $P < 0.05$ ; \*\*\*\*,  $P < 0.0001$ , as determined by two-tailed  
1002 unpaired t-test. (C) Representative images of cholesterol distribution in H $\beta$ CD-treated  
1003 and mock-treated cells are shown. Scale bars, 10  $\mu$ m.

1004

1005 **VIDEO 1, 2, and 3. High-magnification, live-cell microscopy of fluorescent**  
1006 **reovirus virion transport in WT, KO, and KO+ HBMECs.** (1) WT, (2) KO, and (3)  
1007 KO+ cells were adsorbed with Alexa 647-labeled reovirus virions at an MOI of 10,000  
1008 particles/cell at 4°C for 45 min. Fluorescence and brightfield images were captured  
1009 every ~ 25 seconds for 36 min.

1010

1011 **VIDEO 4, 5, and 6. Tracking of fluorescent reovirus virions recruited to a**  
1012 **perinuclear region following entry.** Trajectories of reovirus virions during  
1013 internalization into WT, KO, and KO+ HBMECs from videos 1, 2, and 3 were tracked  
1014 with the spot-tracking plugin function of Icy-Bioimage analysis software (84). Cell  
1015 contour was defined as a region of interest (ROI), and ~ 7 pixels/spot were monitored.  
1016 The colored bar represents the trajectory depending on time, in which each color (from  
1017 yellow to red) corresponds to an interval of ~ 7.5 min in the time-lapse videos. Scale  
1018 bars, 10  $\mu$ m.

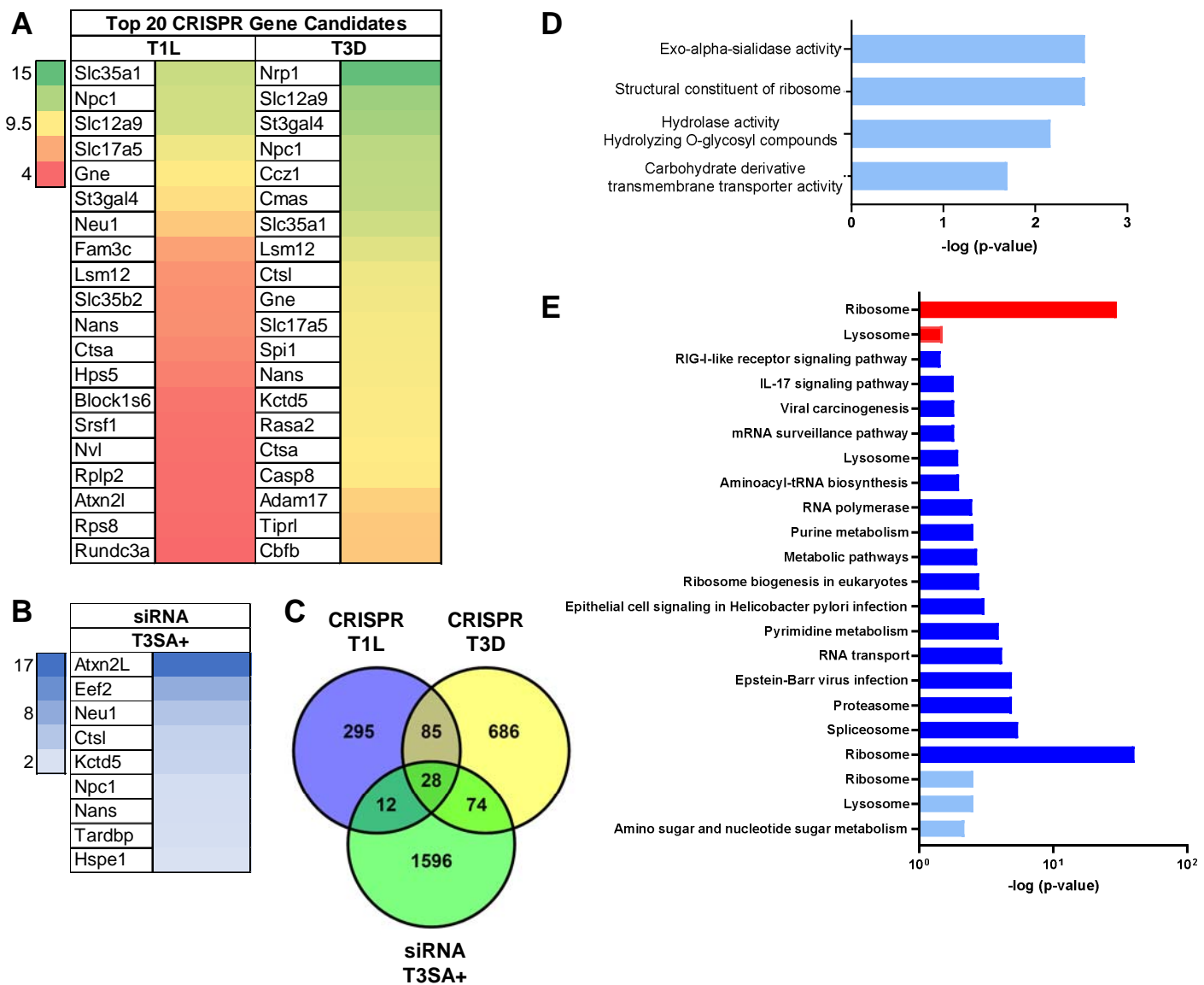


**FIG 1** CRISPR and siRNA screens identify NPC1 as a cellular factor required for reovirus infection. (A) The top 20 candidates from the CRISPR screen using reovirus strains T1L and T3D are ranked by their STAR scores. Heat map indicates STAR values. (B) Genes from the siRNA screen using reovirus strain T3SA+ common to the CRISPR screen using T1L and T3D, excluding ribosomal genes. Heat map indicates z-score values. (C) Venn diagram of genes from the CRISPR screens using T1L and T3D and the siRNA screen using T3SA+. (D) Molecular function pathways using Gene Ontology to analyze genes from the CRISPR screen common to T1L and T3D. (E) KEGG pathways identified for the CRISPR screen using T1L (red) and T3D (blue) and siRNA screen using T3SA+ (light blue).

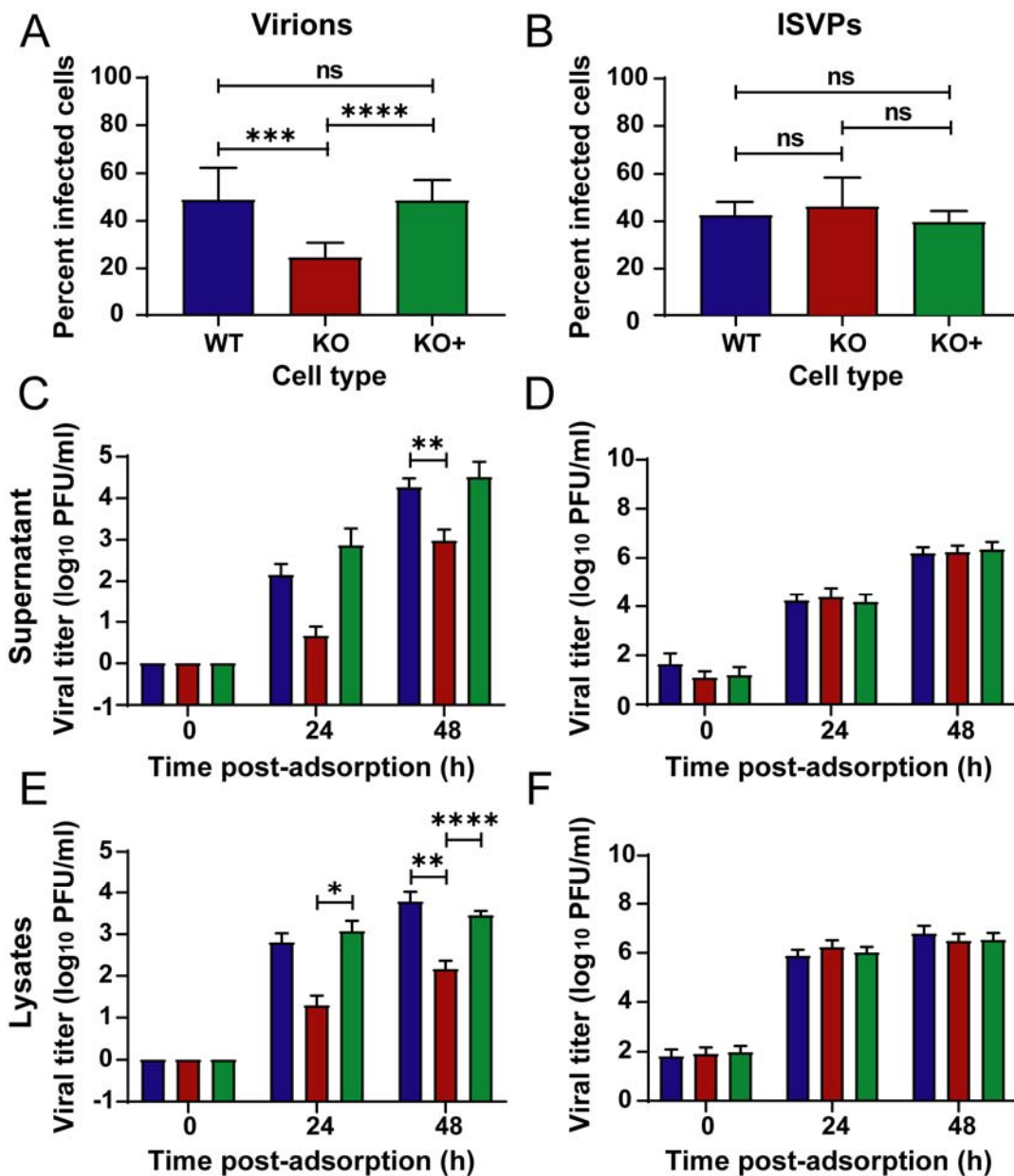


**FIG 2** Viral infectivity and titers following adsorption by reovirus virions and ISVPs. (A, B) WT, KO, and KO+ HBMECs were adsorbed with reovirus (A) virions or (B) ISVPs at MOIs of 10,000 or 100 particles/cell, respectively, and fixed at 18 h post-adsorption. The percentage of infected cells was determined by enumerating reovirus-infected cells following immunostaining with a reovirus-specific antiserum. (C-F) WT, KO, and KO+ cells were adsorbed with reovirus (C, E) virions at an MOI of 1 PFU/cell or (D, F) ISVPs at an MOI of 5 particles/cell. Viral titers in cell-culture supernatants and lysates were determined by plaque assay at 0, 24, and 48 h post-adsorption. The results are presented as the mean of three independent experiments. Error bars indicated standard deviation. \*, P < 0.05; \*\*, P < 0.01; \*\*\*, P < 0.001; \*\*\*\*, P < 0.0001, as determined by t-test.

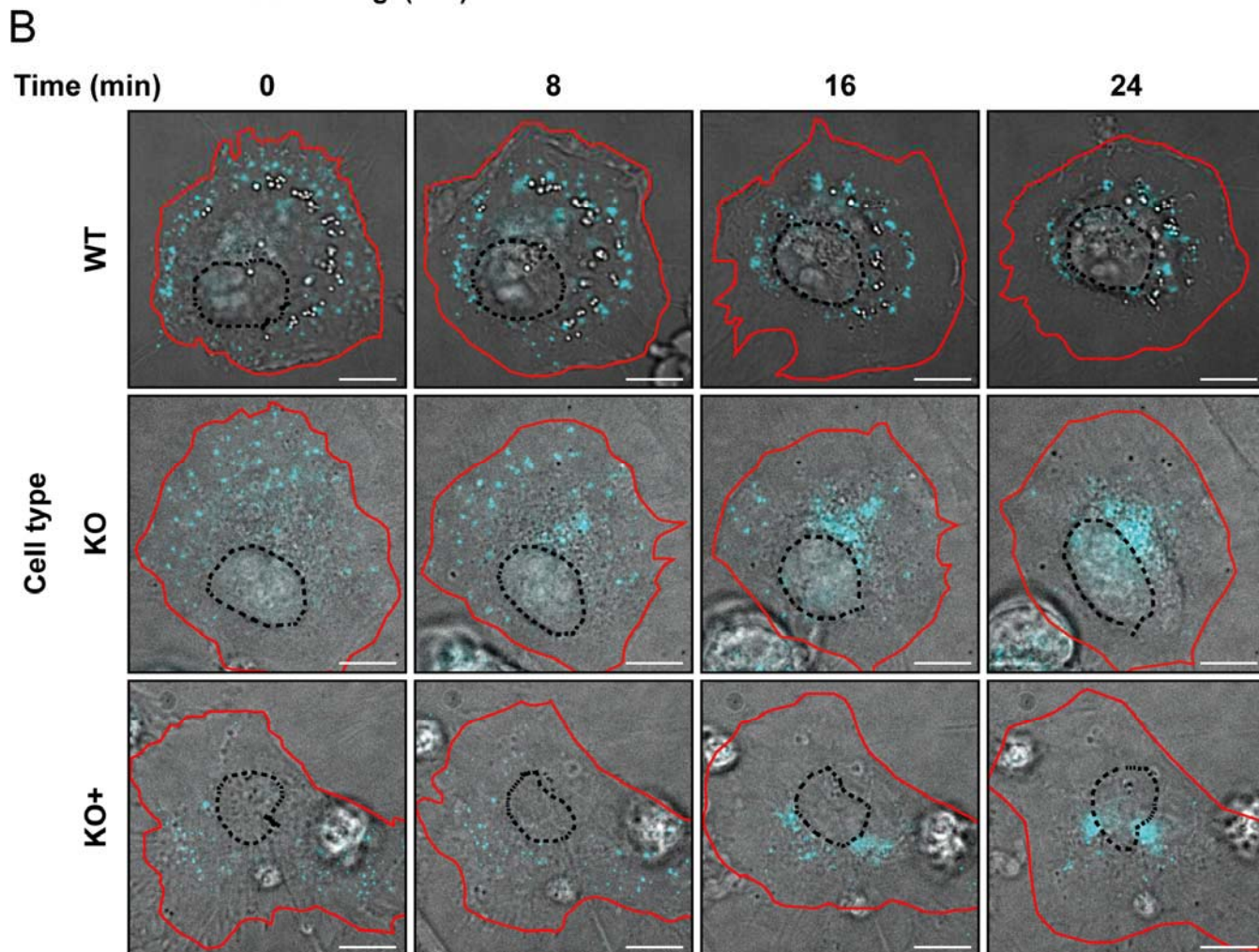
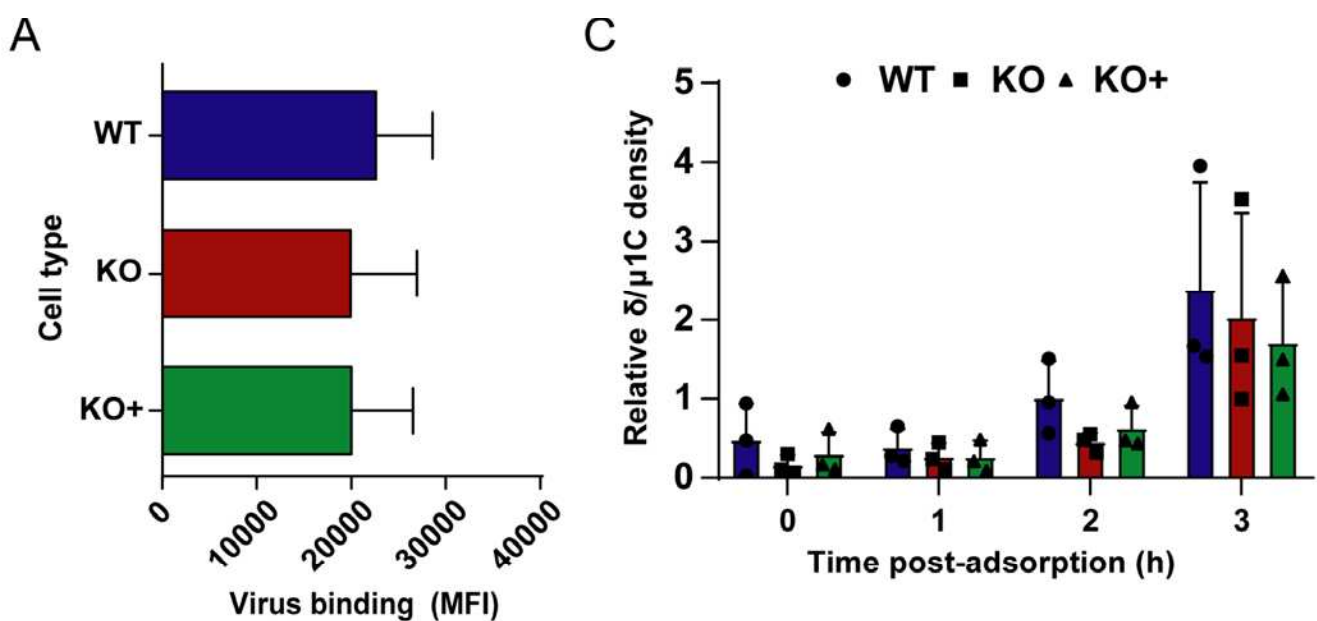


**FIG 3** Binding, internalization, and uncoating are not disrupted by cholesterol accumulation in NPC1 KO HBMECs. (A) WT, KO, and KO+ HBMECs were adsorbed with Alexa 647 labeled-reovirus virions at an MOI of 10,000 particles/cell at 4°C for 1 h, fixed with 1% PFA, and analyzed for virus binding using flow cytometry. The results are presented as mean virus binding as determined by mean fluorescence intensity (MFI) of three independent experiments. Error bars indicated standard deviation. (B) WT, KO, and KO+ HBMECs were adsorbed with Alexa 647 labeled-reovirus virions at an MOI of 10,000 particles/cell at 4°C for 45 min and imaged using high magnification live-cell imaging, with images captured every ~ 25 seconds. Representative micrographs from videos at the indicated intervals are shown. Scale bars, 10  $\mu$ m. (C) WT, KO, and KO+ HBMECs were adsorbed with reovirus virions at an MOI of 10,000 particles/cell at 4°C for 1 h and lysed at the intervals post-adsorption shown. Cell lysates were subjected to electrophoresis and immunoblotting using a reovirus-specific polyclonal rabbit antiserum. The results are presented as the mean ratio of the  $\delta$  and  $\mu 1C$  bands from three independent experiments. Error bars indicate standard deviation. Differences are not significant, as determined by two-tailed unpaired t-test.

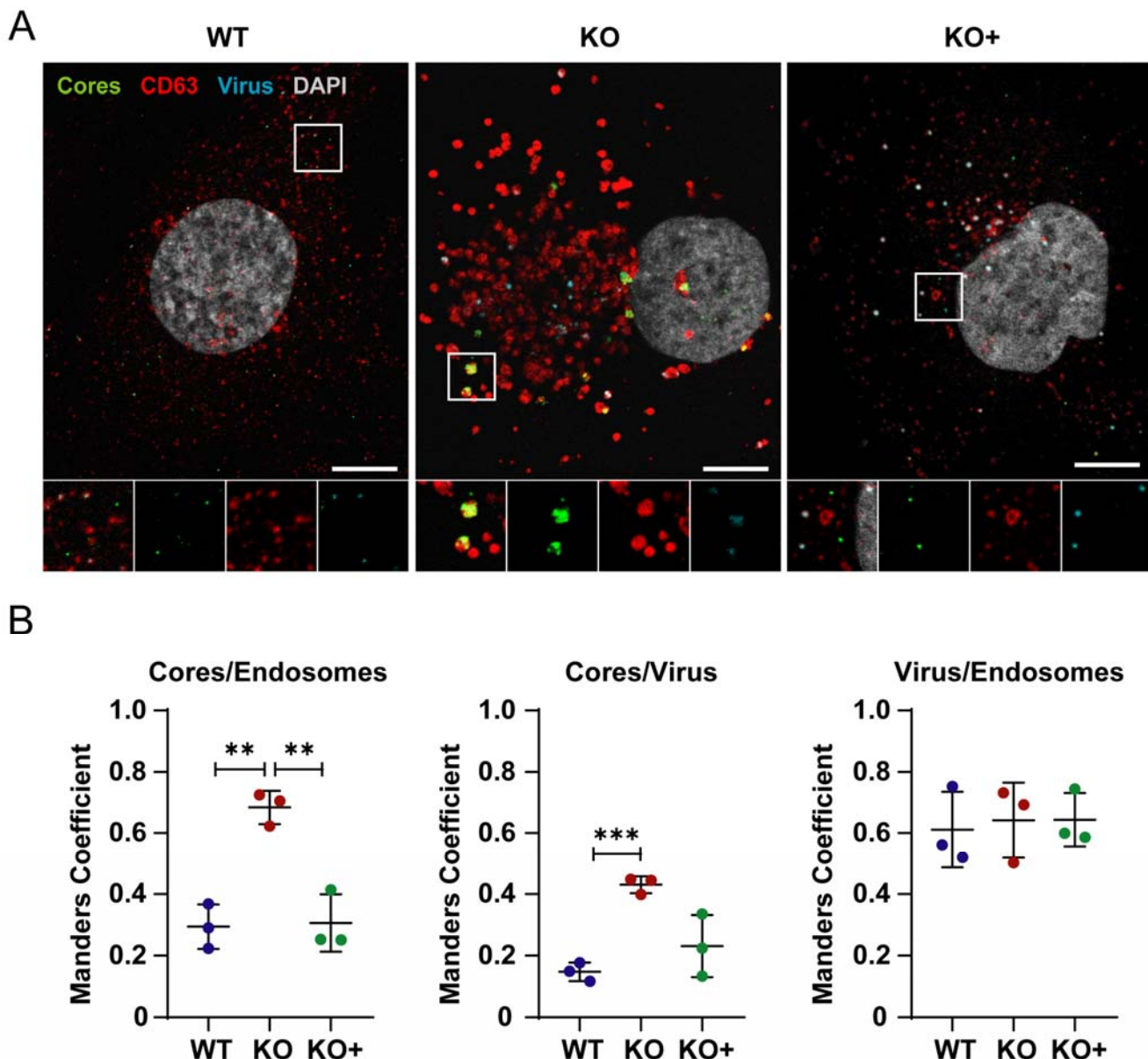


**FIG 4** Cytosolic entry of reovirus cores. (A) WT, KO, and KO+ HBMECs were adsorbed with Alexa 647 labeled-reovirus virions at an MOI of 10,000 particles/cell at 37°C for 45 min and fixed with 4% PFA at 8 h post-adsorption. Cells were stained with DAPI, a CD-63-specific antibody to label endosomes, and an antiserum specific for reovirus cores, and imaged using confocal microscopy. Representative confocal micrographs are shown. (B) Colocalization of reovirus, cores, and endosomes was analyzed using the JaCoP plugin function from ImageJ. The results are presented as the mean colocalization (quantified by Manders coefficient) of ~ 50 cells from three independent experiments. Error bars indicate standard deviation. \*\*,  $P < 0.01$ ; \*\*\*,  $P < 0.001$ , as determined by two-tailed unpaired t-test.

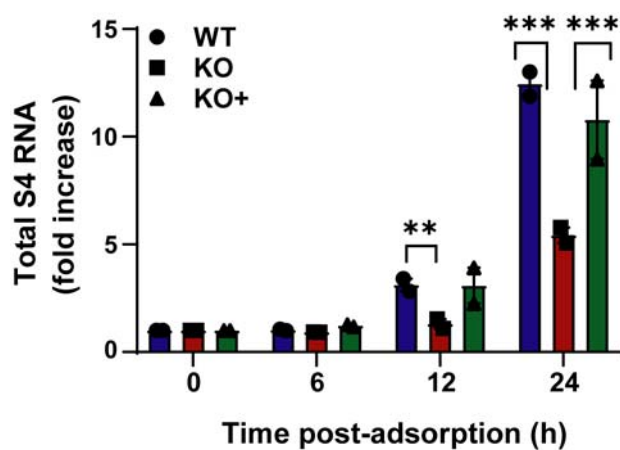


**FIG 5** Synthesis of nascent RNA is reduced in NPC1 KO HBMECs. WT, KO, and KO+ HBMECs were adsorbed with reovirus virions at an MOI of 1 PFU/cell at 37°C for 1 h, lysed at the intervals post-adsorption shown, and assayed for positive-sense reovirus s4 RNA by RT-qPCR. The results are presented as the mean number of copies of reovirus s4 RNA by qPCR from two independent experiments. Error bars indicate standard errors of the mean. \*\*,  $P < 0.01$ ; \*\*\*,  $P < 0.001$ , as determined by t-test.

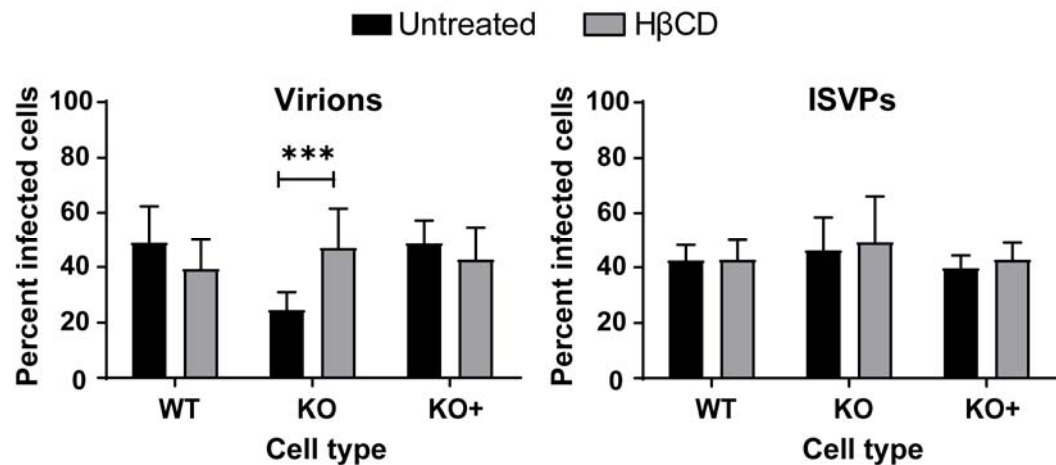


**FIG 6** H $\beta$ CD treatment restores reovirus infection of NPC1 KO HBMECs. WT, KO, and KO+ HBMECs were pretreated with 1 mM H $\beta$ CD or PBS for 24 h, adsorbed with reovirus virions or ISVPs at MOIs of 10,000 or 100 particles/cell, respectively, and fixed at 18 h post-adsorption. The percentage of infected cells was determined by enumerating reovirus-infected cells following immunostaining with a reovirus-specific antiserum. The results are presented as the mean of three independent experiments. Error bars indicated standard deviation. \*\*\*, P < 0.001 as determined by two-tailed unpaired t-test.